NTIS #

SSC-448

FRACTURE MECHANICS CHARACTERIZATION OF ALUMINUM ALLOYS FOR MARINE STRUCTURAL APPLICATIONS

SHIP STRUCTURE COMMITTEE
2007

Ship Structure Committee

RADM Craig E. Bone
U. S. Coast Guard Assistant Commandant,
Marine Safety and Environmental Protection
Chairman, Ship Structure Committee

Mr. W. Thomas Packard
Director,
Survivability and Structural Integrity Group
Naval Sea Systems Command

Dr. Roger Basu
Senior Vice President
American Bureau of Shipping

Mr. Joseph Byrne
Director, Office of Ship Construction
Maritime Administration

Mr. William Nash
Director General, Marine Safety,
Safety & Security
Transport Canada

Mr. Kevin Baetsen
Director of Engineering
Military Sealift Command

Dr. Neil Pegg
Group Leader - Structural Mechanics
Defence Research & Development Canada - Atlantic

CONTRACTING OFFICER TECHNICAL REP.
Mr. Chao Lin / MARAD
Mr. Glenn Ashe / ABS
DRDC / USCG

EXECUTIVE DIRECTOR
Lieutenant Benjamin A. Gates
U. S. Coast Guard

SHIP STRUCTURE SUB-COMMITTEE

AMERICAN BUREAU OF SHIPPING

Mr. Glenn Ashe
Mr. Derek Novak
Mr. Phil Rynn
Mr. Balji Menon

DEFENCE RESEARCH & DEVELOPMENT CANADA ATLANTIC
Dr. David Stredulinsky
Mr. John Porter

MARITIME ADMINISTRATION
Mr. Chao Lin
Mr. Carl Setterstrom
Mr. Richard Sonnenschein

MILITARY SEALIFT COMMAND
Mr. Michael W. Touma
Mr. James Kent
Mr. Paul Handler

ONR / NAVY/ NSWCCD
Dr. Paul Hess
Dr. Jeff Beach
Dr. Yapa Rajapakse
Mr. Allen H. Engle

TRANSPORT CANADA
Mr. Richard Stillwell

US COAST GUARD

Capt. Patrick Little
Mr. H. Paul Cojeen
Mr. Rubin Sheinberg

SOCIETY OF NAVAL ARCHITECTS AND MARINE ENGINEERS
Mr. Jaideep Sirkar
Mr. Al Rowen
Mr. Norman Hammer

Member Agencies:

American Bureau of Shipping
Defence Research Development Canada
Maritime Administration
Military Sealift Command
Naval Sea Systems Command
Society of Naval Architects & Marine Engineers
Transport Canada
United States Coast Guard

Ship
Structure
Committee

Address Correspondence to:

Executive Director
Ship Structure Committee
U.S. Coast Guard (CG-3PSE/SSC)
2100 Second Street, SW
Washington, D.C. 20593-0001
Web site: http://www.shipstructure.org

SSC – 448
SR – 1447

MARCH 21, 2007

FRACTURE MECHANICS CHARACTERIZATION OF ALUMINUM ALLOYS FOR MARINE STRUCTURAL APPLICATIONS

The properties of fatigue crack growth resistance and fracture toughness are required to analyze structural integrity and damage tolerances of aluminum structures. Historically, fatigue crack growth data has usually been altered by external forces and often the results did not accurately represent the true behavior of the material. A new methodology with successful results has been developed to account for these effects and it has been used in this report.

Three aluminum alloys used in marine structural applications: 5083-H321, 5086-H116, and 5383-H116 were investigated. Tests were conducted in air as well as a simulated salt water environment at three different frequencies. This report complements the work completed in SSC – 410, "Fatigue of Aluminum Structural Weldments".

CRAIG E. BONE
Rear Admiral, U.S. Coast Guard
Chairman, Ship Structure Committee

Technical Report Documentation Page

1. Report No. **SSC - 448**	2. Government Accession No.	3. Recipient's Catalog No.	
4. Title and Subtitle Fracture Mechanics Characterization of Aluminum Alloys For Marine Structural Applicatons		5. Report Date **Jan. 1, 2007**	
		6. Performing Organization Code	
7. Author(s) J. Keith Donald		8. Performing Organization Report No. SR-1447	
9. Performing Organization Name and Address Fracture Technology Associates		10. Work Unit No. (TRAIS)	
2412 Emrick Boulevard Bethlehem, PA 18020		11. Contract or Grant No.	
12. Sponsoring Agency Name and Address Ship Structure Committee C/O Commandant (CG-3PSE/SSC) United States Coast Guard 2100 2nd Street, SW Washington, DC 20593-0001		13. Type of Report Final Report	
		14. Sponsoring Agency Code CG - 3P	
15. Supplementary Notes Sponsored by the Ship Structure Committee and its member agencies			
16. Abstract			
17. Key Words	18. Distribution Statement Distribution Available From: National Technical Information Service U.S. Department of Commerce Springfield, VA 22151 Ph. (703) 605-6000		
19. Security Classif. (of this report)	20. Security Classif. (of this page)	21. No. of Pages	22. Price

CONVERSION FACTORS
(Approximate conversions to metric measures)

To convert from	to	Function	Value
LENGTH			
inches	meters	divide	39.3701
inches	millimeters	multiply by	25.4000
feet	meters	divide by	3.2808
VOLUME			
cubic feet	cubic meters	divide by	35.3149
cubic inches	cubic meters	divide by	61,024
SECTION MODULUS			
$inches^2$ $feet^2$	$centimeters^2$ $meters^2$	multiply by	1.9665
$inches^2$ $feet^2$	$centimeters^3$	multiply by	196.6448
$inches^4$	$centimeters^3$	multiply by	16.3871
MOMENT OF INERTIA			
$inches^2$ $feet^2$	$centimeters^2$ meters	divide by	1.6684
$inches^2$ $feet^2$	$centimeters^4$	multiply by	5993.73
$inches^4$	$centimeters^4$	multiply by	41.623
FORCE OR MASS			
long tons	tonne	multiply by	1.0160
long tons	kilograms	multiply by	1016.047
pounds	tonnes	divide by	2204.62
pounds	kilograms	divide by	2.2046
pounds	Newtons	multiply by	4.4482
PRESSURE OR STRESS			
$pounds/inch^2$	$Newtons/meter^2$ (Pascals)	multiply by	6894.757
kilo $pounds/inch^2$	mega $Newtons/meter^2$ (mega Pascals)	multiply by	6.8947
BENDING OR TORQUE			
foot tons	meter tons	divide by	3.2291
foot pounds	kilogram meters	divide by	7.23285
foot pounds	Newton meters	multiply by	1.35582
ENERGY			
foot pounds	Joules	multiply by	1.355826
STRESS INTENSITY			
kilo $pound/inch^2$ $inch^{½}$($ksi\sqrt{in}$)	mega Newton $MNm^{3/2}$	multiply by	1.0998
J-INTEGRAL			
kilo pound/inch	$Joules/mm^2$	multiply by	0.1753
kilo pound/inch	kilo $Joules/m^2$	multiply by	175.3

Table of Contents

List of Tables

List of Figures

Appendices

APPENDIX A: PROCUREMENT AND CHARACTERIZATION OF ALLOYS

APPENDIX B: FCGR METHODOLOGY

APPENDIX C: PHOTOGRAPHS OF TEST SAMPLES

APPENDIX D: INDIVIDUAL FCGR CURVES

APPENDIX E: TABULAR RESULTS – ASTM E647 ANALYSIS

APPENDIX F: INDIVIDUAL J VS. ΔA CURVES

APPENDIX G: LOAD VS. LOAD-LINE DISPLACEMENT PLOTS

APPENDIX H: TABULAR RESULTS – ASTM E1820 ANALYSIS

1.0 Chemistry and Mechanical Properties

1.1 Introduction

The following alloys were procured as 0.5 inch thick plates measuring 24 x 24 inches.

5083 H321 supplied as 5083 H321
5086 H116 supplied as 5086 H32 (to ASTM B209)
5383 H116 supplied as 5383/5083 H116 (to ASTM B209-01)

Dr. Harold Reemsnyder provided a detailed summary in Appendix A.

Dr. Catherine Wong provided metallography analysis on the procured alloys (See Appendix A).

Dirats Laboratories was contracted to provide the following services:

1) 3 chemical analysis (one for each alloy)
2) 18 tensile test results (three alloys, 2 orientations, triplicate tests)
3) 15 compact tension samples for fatigue crack growth rate testing (T-L orientation, five per alloy)
4) 9 compact tension samples for non-linear fracture toughness testing (T-L orientation, three per alloy)

1.2 Test Results

Table 1.2.1 summarizes the chemical analysis for each alloy.

TABLE 1.2.1--*Summary of Chemical Analysis*

Test ID	Material	Al %	Cr %	Cu %	Fe %	Mg %	Mn %	Si %	Ti %	Zn %	Zr %
5083-C-1	5083-H321	Rem.	0.08	0.06	0.31	4.82	0.50	0.15	0.03	0.09	--
5086-C-1	5086-H116	Rem.	0.19	0.07	0.31	3.79	0.45	0.14	0.03	0.03	--
5383-C-1	5383-H116	Rem.	0.10	0.06	0.29	4.76	0.53	0.13	0.03	0.08	0.01

Table 1.2.2 summarizes the mechanical properties for each alloy.

TABLE 1.2.2--*Summary of Mechanical Properties*

Temperature: Room Temperature

Test ID	Material	Orientation	0.2%Yield Strength (ksi)	Tensile Strength (ksi)	Elongation %	Reduction of Area %
5083-L-1	5083-H321	L	37.8	52.3	12.1	21.1
5083-L-2	5083-H321	L	37.8	53.0	14.3	20.5
5083-L-3	5083-H321	L	38.2	52.8	16.8	22.4
Average			**37.9**	**52.7**	**14.4**	**21.3**
5083-T-1	5083-H321	T	34.3	52.0	21.5	36.9
5083-T-2	5083-H321	T	34.4	51.6	19.0	34.6
5083-T-3	5083-H321	T	34.3	51.8	18.4	36.8
Average			**34.3**	**51.8**	**19.6**	**36.1**
5086-L-1	5086-H116	L	27.0	45.8	14.8	17.4
5086-L-2	5086-H116	L	26.9	45.7	15.1	16.8
5086-L-3	5086-H116	L	27.0	46.0	15.3	16.1
Average			**27.0**	**45.8**	**15.1**	**16.8**
5086-T-1	5086-H116	T	27.0	45.7	17.1	27.4
5086-T-2	5086-H116	T	26.9	46.2	21.1	36.6
5086-T-3	5086-H116	T	27.1	46.1	19.9	38.7
Average			**27.0**	**46.0**	**19.4**	**34.2**
5383-L-1	5383-H116	L	39.3	54.4	14.1	16.2
5383-L-2	5383-H116	L	39.2	54.1	14.4	17.2
5383-L-3	5383-H116	L	39.0	54.0	12.9	15.6
Average			**39.2**	**54.2**	**13.8**	**16.3**
5383-T-1	5383-H116	T	35.4	53.0	17.5	35.0
5383-T-2	5383-H116	T	35.4	53.5	16.4	24.8
5383-T-3	5383-H116	T	35.5	53.3	18.1	23.3
Average			**35.4**	**53.3**	**17.3**	**27.7**

2.0 Fatigue Crack Growth Rate Characterization

2.1 Introduction

Fatigue crack growth rate (FCGR) testing was conducted on three grades of aluminum alloys designated 5083-H321, 5086-H116 and 5383-H116. A compact tension sample having a width of 4.000 inches and a thickness of 0.500 inches was chosen for all FCGR testing. For each grade of material, two replicate tests were conducted in laboratory air at room temperature and two replicate tests were conducted in simulated ocean water per ASTM Standard D 1141. All samples were machined in the T-L orientation and all testing was conducted using a stress ratio (R) of 0.1. A baseline test frequency of 10 Hz was selected for the laboratory air tests with a baseline frequency of 5 Hz selected for the tests conducted in seawater. Some data were generated in seawater at 0.5 and 0.05 Hz to evaluate frequency sensitivity. The testing was performed in accordance with the requirements of ASTM E647-00 "Standard Test Method for Fatigue Crack Growth Rates". Background information on the methodology for testing and analysis is given in Appendix B.

2.2 Test Equipment

The tests were conducted on two MTS load frames equipped with a 5,000 lbf load cell. Each test frame and controller was interfaced to an Adwin-Gold FTA computer system. The crack length was monitored continuously using the compliance technique enabling the stress intensity to be precisely controlled as a function of crack length. An MTS model 632.03E-20 clip gage with a gage length of 0.475 inches and a working range of 0.100 inches was used for displacement measurement. Fixture alignment was verified for the compact tension clevises by applying a force on a dummy sample and measuring the distance between the loading pins on the front face and back face of the clevis. If the spacing differed by more than 0.001 inches, the clevises were shimmed to bring that difference to within tolerance. Compliance measurement accuracy was enhanced by mounting needle bearings in both the clevis holes and the specimen holes to minimize non-linearity in the load-displacement signal due to pin friction. In addition to improving the accuracy of crack growth measurements, this procedure is considered essential for accurate crack closure measurement. Laboratory temperature and relative humidity were controlled to 75°F +/- 2°F and 40% +/- 5% R.H. throughout the entire period of testing. Photographs of the test equipment and a close-up of a compact tension sample and test fixtures are shown in Figure 2.2.1.

For the synthetic sea-water environment, one gallon of distilled water was combined with a sea-salt mix according to the ASTM D 1141 standard. A peristaltic pump was used to aerate the solution and transfer the environment to the test sample. Custom made clear plastic environment chambers were attached to the test sample with silicon adhesive. These chambers were attached to the sample 24 hours prior to testing to allow a complete cure of the adhesive. A small hole was drilled in the notch to provide flow from one side of the sample to the other. A larger hole was also drilled in the notch and filled with sealant to provide a water-tight seal. The set-up included an air bleed so that the crack remained fully immersed in solution during the entire test. pH readings were recorded daily with a typical range of 8.4 to 7.8. Photographs of the test set-up for the seawater environment are shown in Figure 2.2.2.

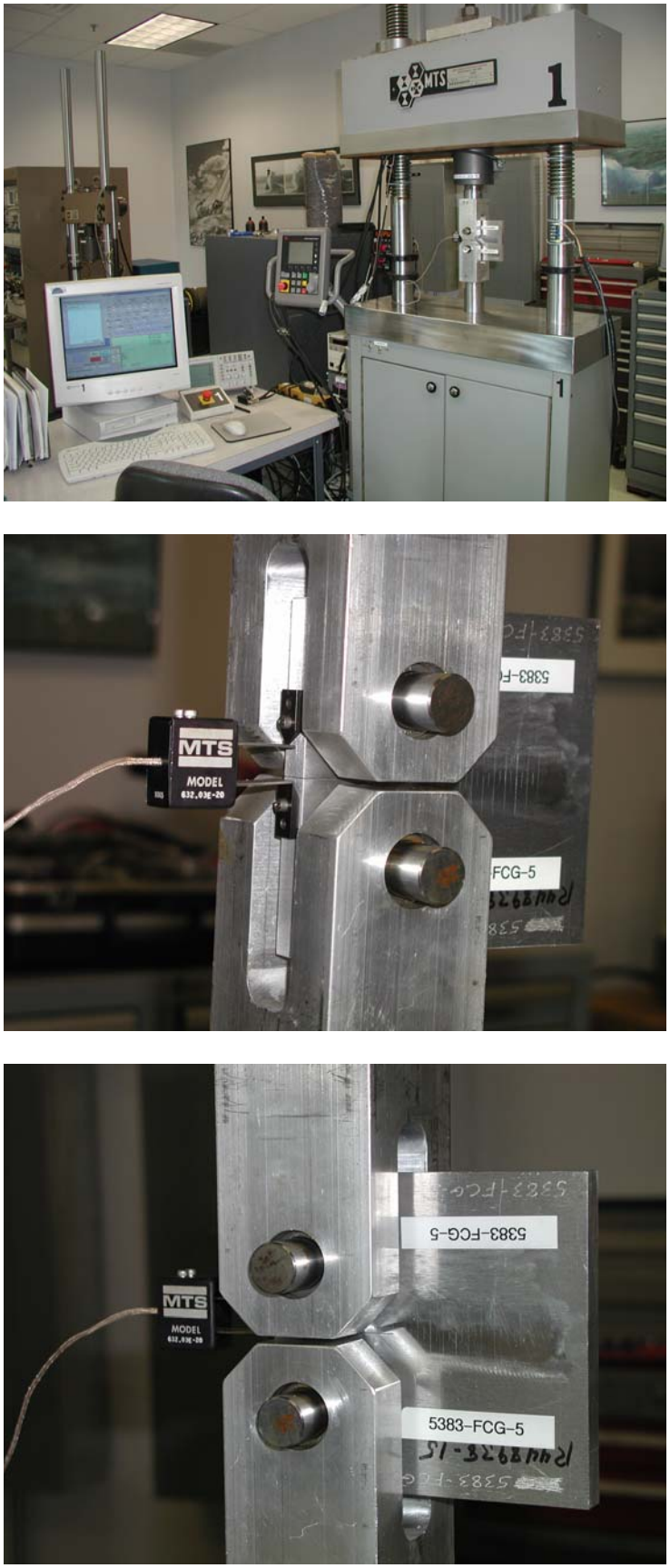

FIGURE 2.2.1: Photographs of test equipment and test set-up (laboratory air environment).

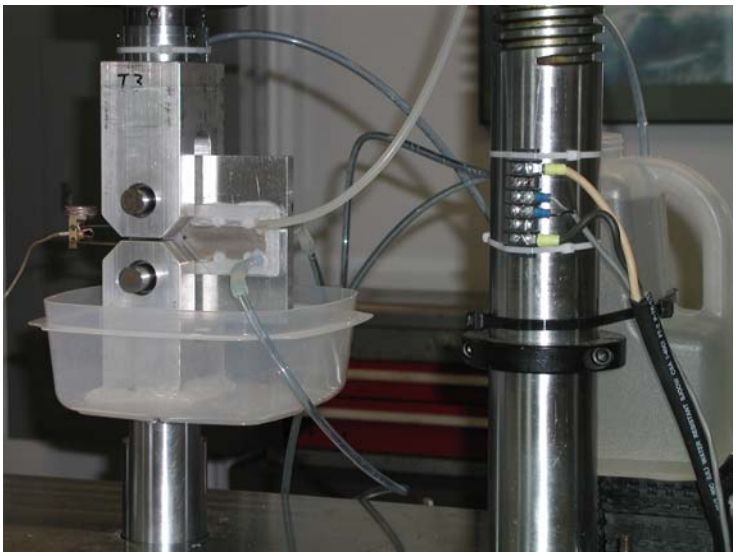

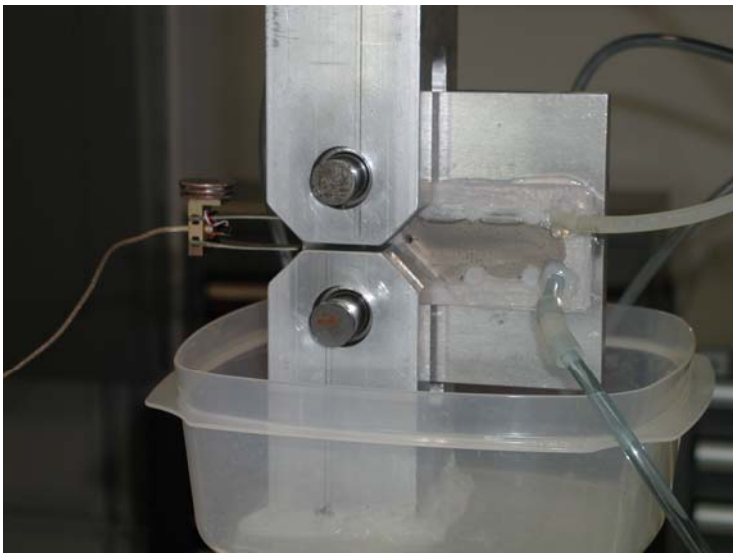

FIGURE 2.2.2: Photographs of test equipment and test set-up (seawater environment).

2.3 Sample Preparation

The test samples were machined according to Figure 2.3.1. After machining the blanks to the final dimensions, but before machining the notch, reference scribes were placed on the edge of the sample spanning the location of the notch. The distance between these scribes was measured to a precision of ±0.0001 inches, both before and after machining the notch. This information was used to estimate the magnitude of residual K at the notch tip due to residual stress. Table 2.5.1 provides a summary of these calculations.

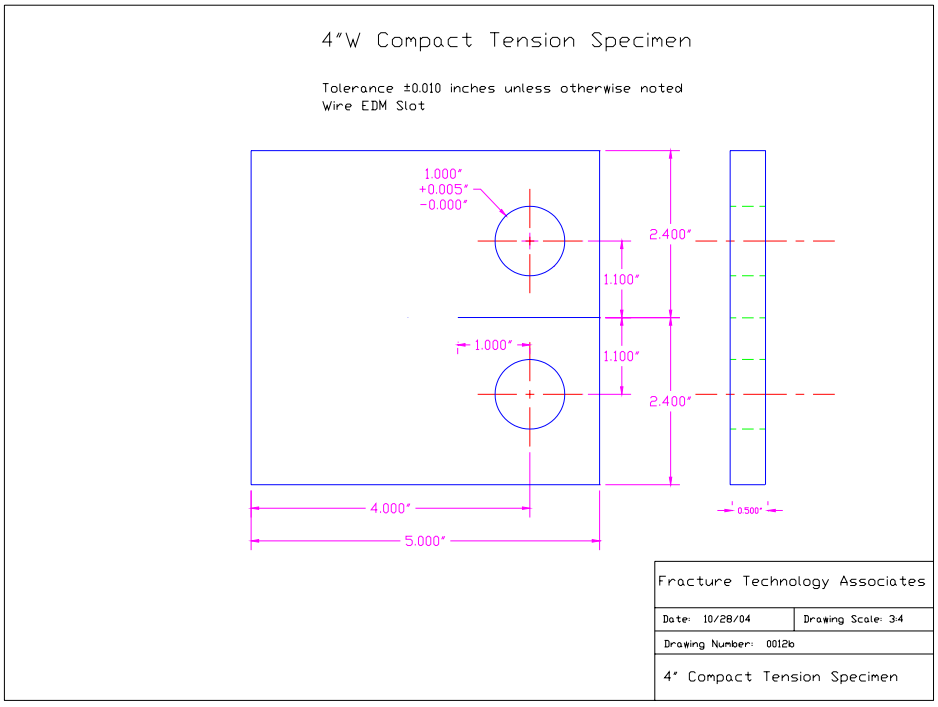

FIGURE 2.3.1: Diagram of C(T) sample for fatigue crack growth testing
(diagram reproduction not to scale)

2.4 Test Procedure

The precracking was initiated at low values of K_{max} (~ 4 ksi√in) in order to initiate a crack at low growth rates. Once initiation was detected and crack evenness was verified, the precracking was continued using a decreasing K-gradient of –4.0 1/inch until a crack growth rate of ~8 x 10^{-8} inch/cycle was achieved. At the completion of precracking, the test was switched to an increasing K-gradient of +4.0 1/inch and continued at that K-gradient until a crack growth rate of 1 x 10^{-5} inch/cycle. A more shallow K-gradient of +2.0 1/in was selected for upper region II (up to 1 x 10^{-4} inch/cycle). Region III crack growth rate data were generated under constant amplitude loading.

Periodic visual measurements of the crack length from each surface were recorded. These measurements, along with the corresponding normalized compliance (EvB/P), were entered into the post-test analysis software to correct for any discrepancy between the physical crack length and the compliance calculated crack length. The cover page of each test (Appendix E) includes a summary of errors between the physical and compliance calculated crack length as well as an adjustment factor (CAF) to the modulus of elasticity to minimize these errors. Compliance coefficients were selected from the ASTM E647 standard based on a clip gage location at the edge of the sample.

For the near-threshold tests, crack growth rate data were generated using a decreasing K-gradient of –4.0 1/in and continued until crack growth rates were less than ~4 x 10^{-9} inch/cycle. After establishing threshold, the tests were continued using an increasing K-gradient of +4.0 1/inch and continued at that K-gradient until a crack growth rate of 1 x 10^{-5} inch/cycle. Both decreasing and increasing K data were generated in laboratory air at a cyclic test frequency of 24 Hz.

During testing, the FTA testing software calculated the effective stress intensity according to the ASTM opening load method. However, another methodology for determining the effective stress intensity was also used and is called the adjusted compliance ratio (ACR) method. Crack growth rates are computed using a combination of the modified secant method and the seven point incremental polynomial technique. The first method is computed as follows:

$$da/dN = (a_{i+2}-a_i)/(N_{i+2}-N_i) \quad (1)$$

and

$$a_{average} = (a_{i+2}+a_i)/2 \quad (2)$$

The second method is thoroughly described in Appendix X1 of ASTM E647. This method smoothes the data but misses three points at the beginning and three points at the end of the data set. The combined methods use the seven-point method for the bulk of the data with the modified secant method used for the “missed” points in the beginning and end of the data set.

2.5 Test Results and Discussion

Table 2.5.1 summarizes the calculation of K residual at the notch tip using the restoring force model. Table 2.5.2 summarizes key test conditions and the cyclic stress intensity at threshold (ΔK_{th}). Threshold determinations were made by applying the data fit as per ASTM E647.

The results of the K residual evaluation (Table 2.5.1) showed mostly tensile residual stress at the notch tip. However, the magnitude of the residual stress was small so no attempt was made to account for residual stress in the analysis.

All samples met the crack front evenness requirement according to ASTM E647. All other validity requirements were satisfied as well.

The following files are available.

***.dat files:**

This file is produced by the analysis software and can be exported to Excel or Grapher for plotting or further analysis. For each data point, the following variables are tabulated:

Description	Units
Index number	
Maximum force	(lbf)
Cyclic force	(lbf)
Normalized compliance	(EvB/P)
Crack length	(in)
Cycle count	
Crack growth rate	(inch/cycle)
K_{max}	(ksi$\sqrt{}$in)
$\Delta K_{applied}$	(ksi$\sqrt{}$in)
$\Delta K_{effective}$ (2% offset opening load method)	(ksi$\sqrt{}$in)
$\Delta K_{effective}$ (ACR method)	(ksi$\sqrt{}$in)
$\Delta K_{effective}$ (2/π partial closure model)	(ksi$\sqrt{}$in)

***.prn files:**

These files include tabular results and additional information such as sample dimensions and visual observation (Appendix E).

A series of plots have been prepared to facilitate the investigation of reproducibility, environment, material, frequency, threshold and crack closure.

2.5.1 Reproducibility

Figures 2.5.1 through 2.5.6 show duplicate test results in both laboratory air and seawater for each grade of material. Agreement is excellent within identical test conditions. For simplicity, the comparisons among the various materials, environments, etc. are made with only one of the duplicate tests.

2.5.2 Effect of Environment

Figures 2.5.7 through 2.5.9 show the effect of environment for each grade of material. The impact is greater at lower growth rates. The crack growth rates may be too fast at the higher growth rates for significant environmental effects. It appears that the environmental effect is greater with the 5083-H321 and 5383-H116 alloy.

2.5.3 Effect of Material

Figures 2.5.10 and 2.5.11 show the effect of the grade of material in laboratory air and seawater respectively. The difference in laboratory air is negligible (Figure 2.5.10). Figure 2.5.11 shows slightly superior performance with the 5086-H116 alloy.

2.5.4 Effect of Frequency

In order to assess the effect of frequency on the FCGR tests conducted in seawater, one sample of each grade of material was tested at three different frequencies (5.0 Hz, 0.5Hz and 0.05Hz). At a frequency of 0.05 Hz both a sineusoidal waveform shape and a hold at maximum load were investigated. For the dwell segment, the waveform consisted of an unload in one second, a reload in one second followed by a hold at maximum load for eighteen seconds. Figures 2.5.12 through 2.5.14 show the effect of the frequency for each grade of material in seawater. The effect of frequency was investigated at crack growth rates of ~1-2 x 10^{-6}, ~1-2 x 10^{-5}, and ~1-2 x 10^{-4} inch/cycle. Almost no frequency effect was observed despite a change of two orders of magnitude in frequency. In fact, at growth rates of ~1-2 x 10^{-5} the crack growth rates at 0.05 Hz appeared to be slower, not faster, as would be expected. This behavior suggests that these alloys are fairly resistant to corrosion fatigue in seawater.

2.5.5 Threshold Behavior

Figure 2.5.15 shows a comparison of the threshold data for each grade of material. Good agreement was noted where the decreasing and increasing K data overlap. The increasing K data are in good agreement with the previous test data in laboratory air. However, the decreasing K threshold data appear higher then would have been expected from the results of the standard increasing K tests. An examination of the threshold fatigue surfaces indicates darker appearance most likely associated with crack closure contact. The size of the sample and the long crack length are not generally recommended for threshold testing and this may in part explain the some deviation in behavior just above the knee of the curve. This difference is clearly illustrated in Figures 2.5.16 through 2.5.18.

2.5.6 Effect of Crack Closure

In order to properly interpret the results of standard fatigue crack growth tests it is often necessary to incorporate corrective techniques to the ΔK applied data. Since Elber discovered the existence of crack closure, it has become a widely used tool to explain the extrinsic response of fatigue crack growth rate behavior. Crack closure is a crack tip shielding mechanism whereby the crack-tip cyclic strain is partially shielded from damaging stress. The source of this shielding is most commonly caused by crack wake interference due to plasticity, roughness (micro-structure), oxide and/or residual stress. The experimental measurement of crack closure has been hampered by widely varying and non-repeatable methods of evaluation. Furthermore, experimental observations are subject to varying and inconsistent methods of interpretation. In an attempt to improve consistency of measurement, ASTM E647 has an automated offset opening load technique. After two round-robin programs, this method was adopted as an annex to the ASTM E647 standard. However, this method often over corrects the ΔK applied data primarily because the method fails to account for evidence of crack tip cyclic strain below the opening load. This is especially important if the closure mechanism is not necessarily near the crack tip but distributed along the full wake of the crack.

As an alternative approach, the adjusted compliance ratio (ACR) method of determining the effective stress intensity has been useful in accounting for compressive residual stress and other sources of remote closure resulting in an intrinsic FCGR curve that is thought to emulate the small crack behavior. The method uses the same load-displacement records as the opening load method, but it accounts for partial closure effects (effects below the opening load). Further details of this methodology are provided in Appendix B.

The data from Figures 2.5.7 through 2.5.9 have been re-plotted in Figures 2.5.19 through 2.5.21 using the ACR method to estimate ΔK_{eff}. These plots show that in the absence of remote closure, the seawater environment has an equivalent or possibly even greater impact of the FCGR behavior. Depending on exposure times, crack size and crack growth rates, the extrinsic behavior (based on $\Delta K_{applied}$) may be different than the intrinsic behavior based on $\Delta K_{effective}$. This is because the environment can work in two ways. It tends to accelerate crack growth due to environmental influence at the crack tip. At the same time it can lead to suppressed crack growth rates due to corrosion product build-up resulting in crack closure shielding in the crack wake. By analyzing the effective stress intensity, the two opposing mechanisms can be partitioned.

A re-examination of the data from Figure 2.5.10 shows that when crack closure is accounted for, there is even less difference in the three grades of material (Figure 2.5.22). Similarly, in seawater, (Figure 2.5.11) some of the perceived differences in lower region II data may be attributed to crack closure as well (Figure 2.5.23). Finally, a re-examination of the near-threshold data from Figure 2.5.15 also shows that the intrinsic behavior of all three alloys is nearly identical (Figure 2.5.24).

TABLE 2.5.1—*Estimation of K Residual Using Restoring Force Model*

Test ID	Notch Mouth Displacement Change (inches)	$K_{residual}$ (ksi√in)
5083-1	+0.0002	+0.12
5083-2	+0.0001	+0.06
5083-3	+0.0004	+0.24
5083-4	+0.0004	+0.24
5083-5	+0.0001	+0.06
5086-1	+0.0002	+0.12
5086-2	+0.0000	+0.00
5086-3	+0.0002	+0.12
5086-4	+0.0001	+0.06
5086-5	+0.0000	+0.00
5383-1	+0.0000	+0.00
5383-2	+0.0001	+0.06
5383-3	+0.0000	+0.00
5383-4	-0.0001	-0.06
5383-5	+0.0001	+0.06

TABLE 2.5.2—*Summary of Fatigue Crack Growth Test Conditions and Results*

Temperature: **75 deg F**
Stress Ratio: **0.1**
Orientation: **T-L**

Test ID	Material	Environment	K-Gradient (1/in)	Freq. (Hz)	ΔK_{th} (ksi$\sqrt{in}$)
5083-1B	5083-H321	Air	+4.0	10.0	--
5083-1C	5083-H321	Air	+2.0	10.0	--
5083-1D	5083-H321	Air	Constant Load	5.0	--
5083-2B	5083-H321	Air	+4.0	10.0	--
5083-2C	5083-H321	Air	+2.0	10.0	--
5083-2D	5083-H321	Air	Constant Load	5.0	--
5083-3B	5083-H321	Seawater	+4.0	5.0	--
5083-3C	5083-H321	Seawater	+2.0	5.0	--
5083-3D	5083-H321	Seawater	Constant Load	5.0	--
5083-4B	5083-H321	Seawater	+4.0	5.0, 0.5	--
5083-4C	5083-H321	Seawater	+2.0	5.0, 0.5, 0.05	--
5083-4D	5083-H321	Seawater	Constant Load	5.0, 0.5, 0.05	--
5083-5A	5083-H321	Air	-4.0	24.0	2.64
5083-5B	5083-H321	Air	+4.0	24.0	--
5086-1B	5086-H116	Air	+4.0	10.0	--
5086-1C	5086-H116	Air	+2.0	10.0	--
5086-1D	5086-H116	Air	Constant Load	5.0	--
5086-2B	5086-H116	Air	+4.0	10.0	--
5086-2C	5086-H116	Air	+2.0	10.0	--
5086-2D	5086-H116	Air	Constant Load	5.0	--
5086-3B	5086-H116	Seawater	+4.0	5.0	--
5086-3C	5086-H116	Seawater	+2.0	5.0	--
5086-3D	5086-H116	Seawater	Constant Load	5.0	--
5086-4B	5086-H116	Seawater	+4.0	5.0, 0.5	--
5086-4C	5086-H116	Seawater	+2.0	5.0, 0.5, 0.05	--
5086-4D	5086-H116	Seawater	Constant Load	5.0, 0.5, 0.05	--
5086-5A	5086-H116	Air	-4.0	24.0	3.01
5086-5B	5086-H116	Air	+4.0	24.0	--

TABLE 2.5.2—*Summary of Test Conditions (continued)*
Temperature: 75 deg F
Stress Ratio: 0.1
Orientation: T-L

Test ID	Material	Environment	K-Gradient (1/in)	Freq. (Hz)	ΔK_{th} (ksi$\sqrt{in}$)
5383-1B	5383-H116	Air	+4.0	10.0	--
5383-1C	5383-H116	Air	+2.0	10.0	--
5383-1D	5383-H116	Air	Constant Load	5.0	--
5383-2B	5383-H116	Air	+4.0	10.0	--
5383-2C	5383-H116	Air	+2.0	10.0	--
5383-2D	5383-H116	Air	Constant Load	5.0	--
5383-3B	5383-H116	Seawater	+4.0	5.0	--
5383-3C	5383-H116	Seawater	+2.0	5.0	--
5383-3D	5383-H116	Seawater	Constant Load	5.0	--
5383-4B	5383-H116	Seawater	+4.0	5.0, 0.5	--
5383-4C	5383-H116	Seawater	+2.0	5.0, 0.5, 0.05	--
5383-4D	5383-H116	Seawater	Constant Load	5.0, 0.5, 0.05	--
5383-5A	5383-H116	Air	-4.0	24.0	2.67
5383-5B	5383-H116	Air	+4.0	24.0	--

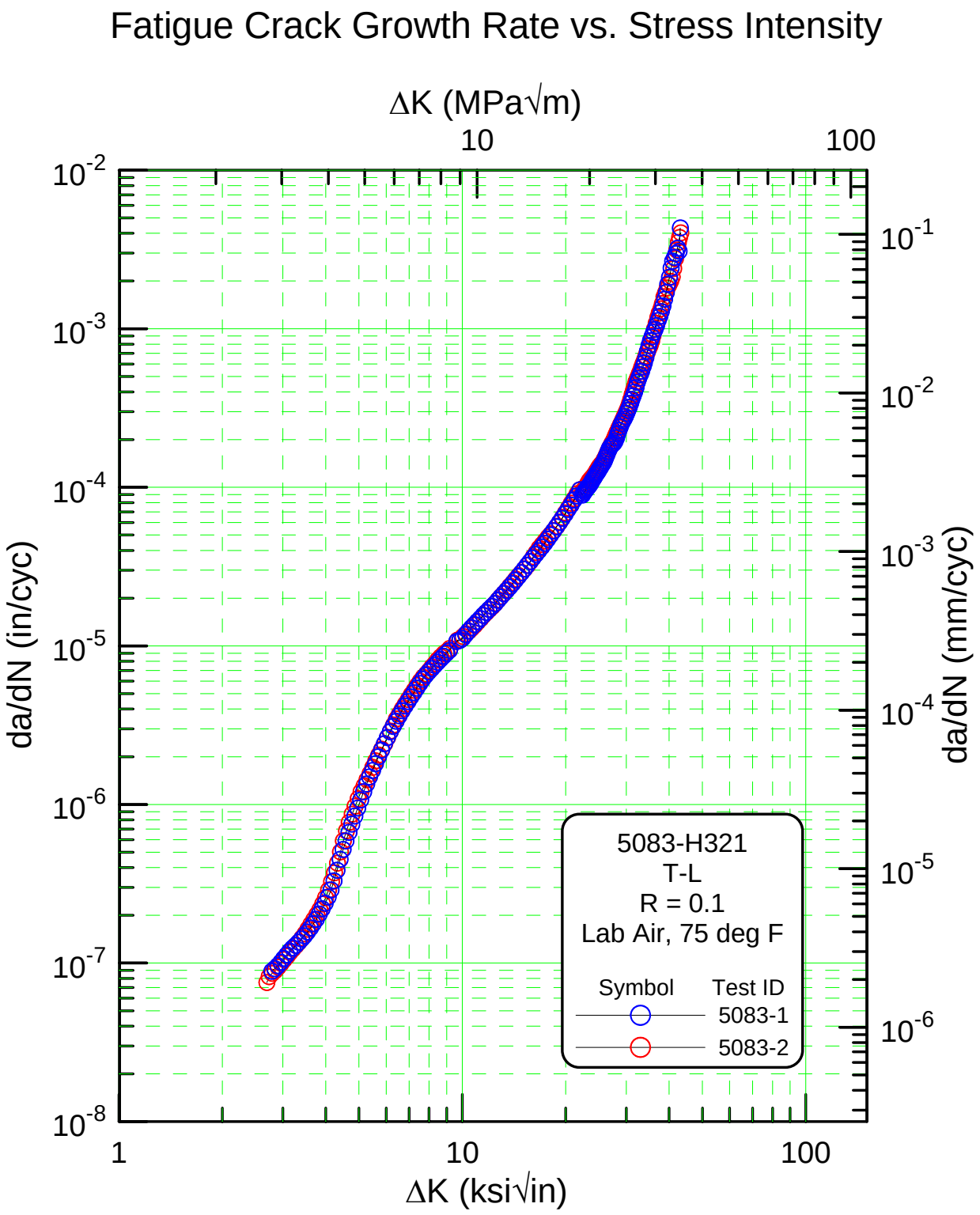

FIGURE 2.5.1: FCGR response comparing duplicate tests for the 5083-H321 alloy in laboratory air.

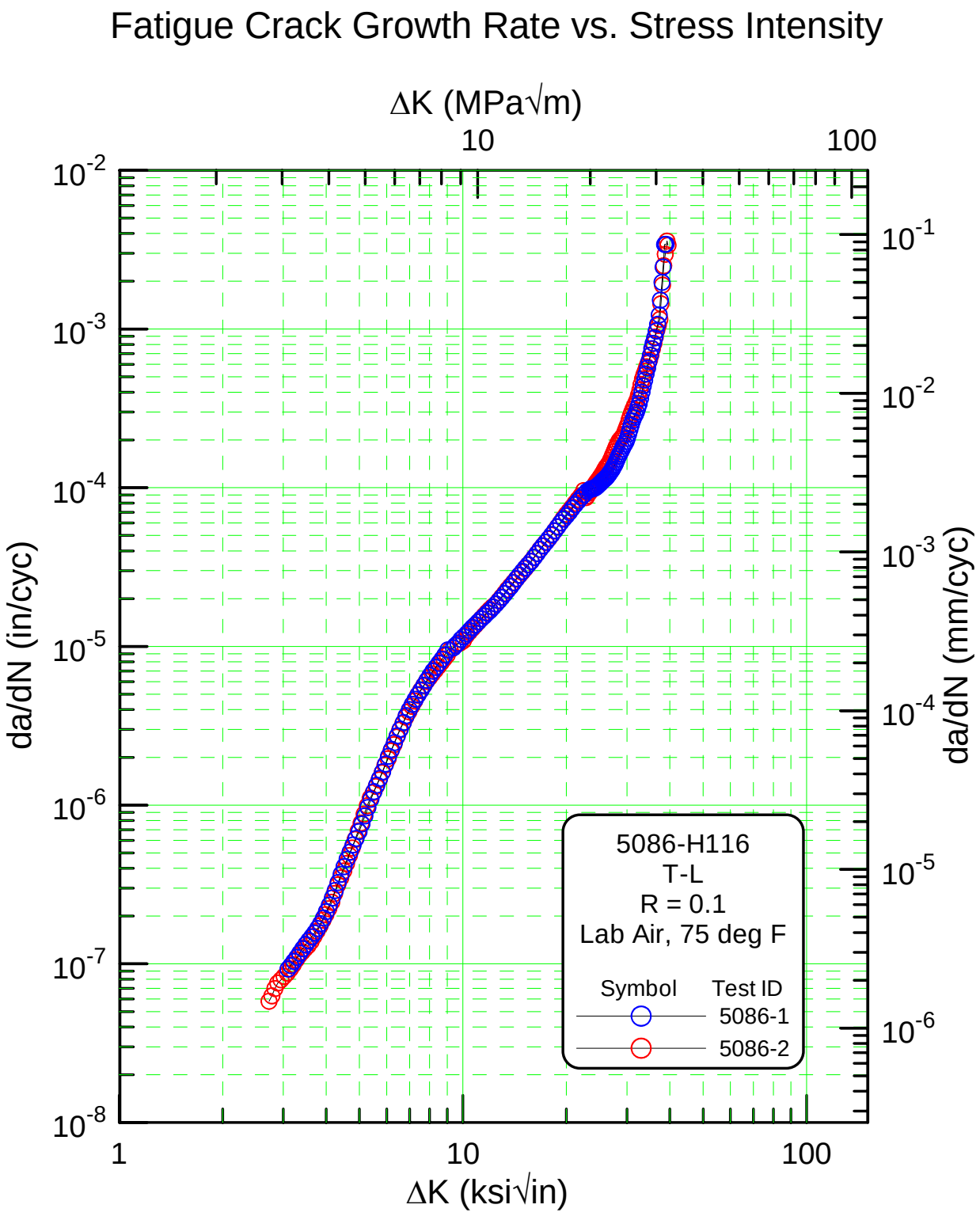

FIGURE 2.5.2: FCGR response comparing duplicate tests for the 5086-H116 alloy in laboratory air.

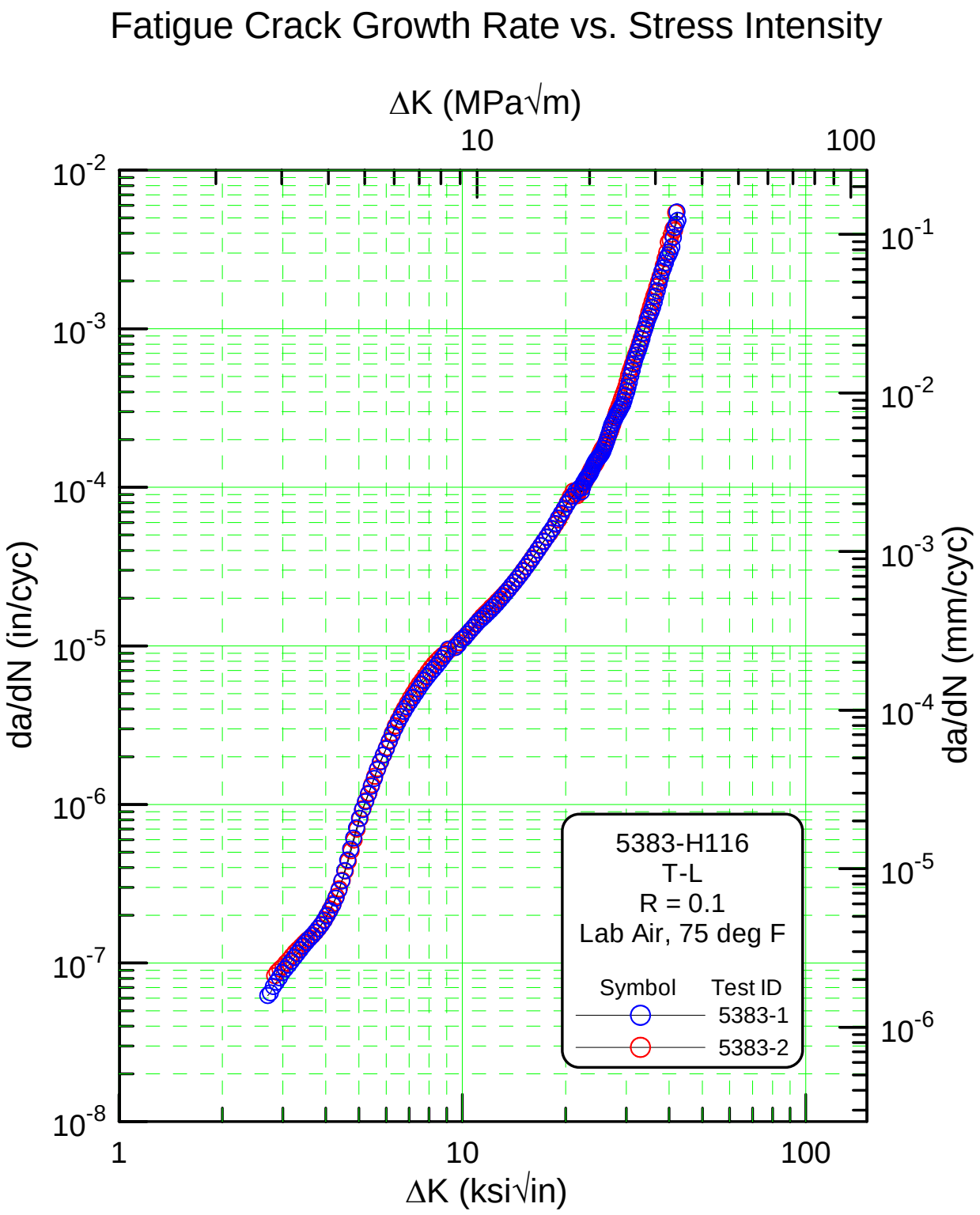

FIGURE 2.5.3: FCGR response comparing duplicate tests for the 5383-H116 alloy in laboratory air.

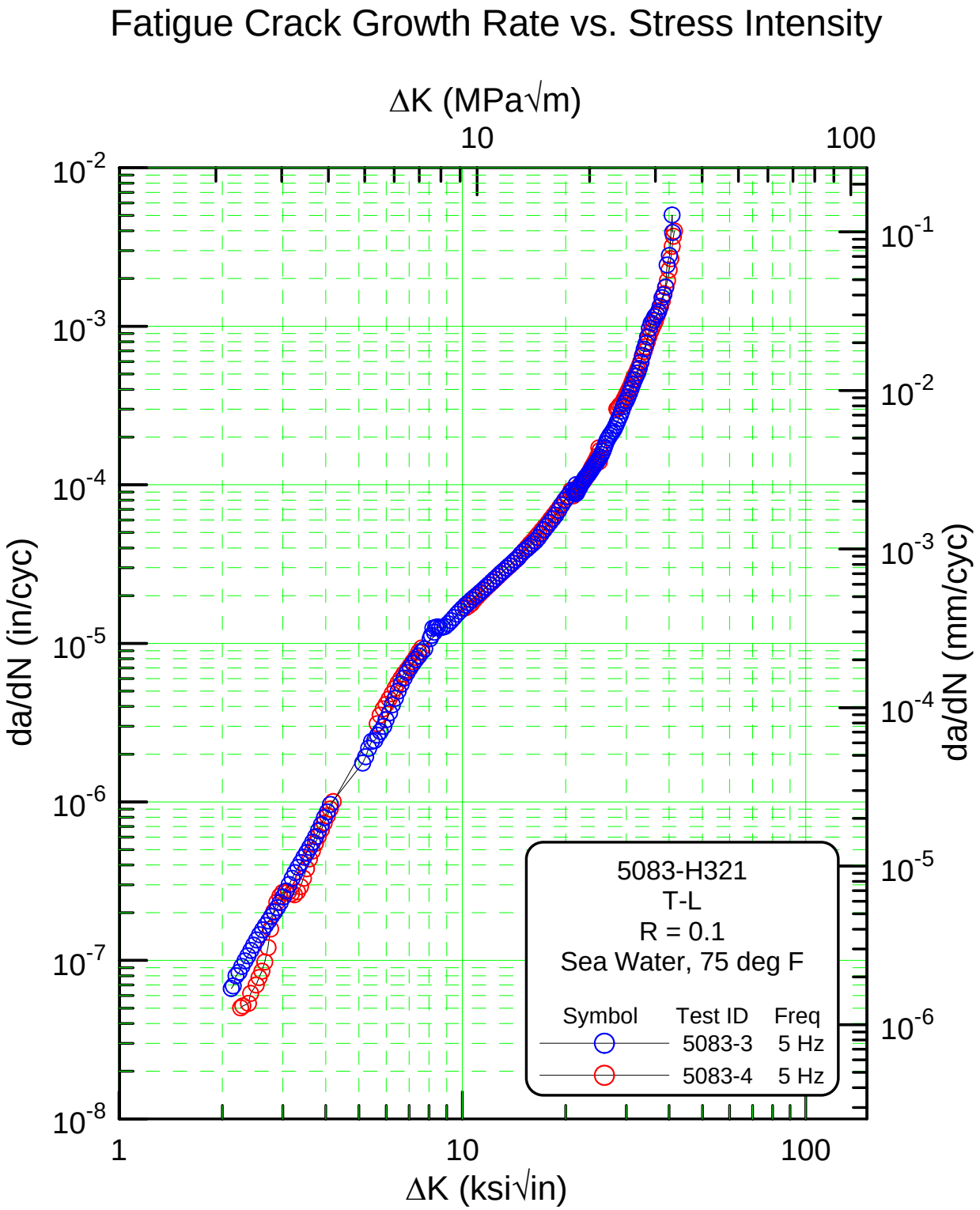

FIGURE 2.5.4: FCGR response comparing duplicate tests for the 5083-H321 alloy in seawater.

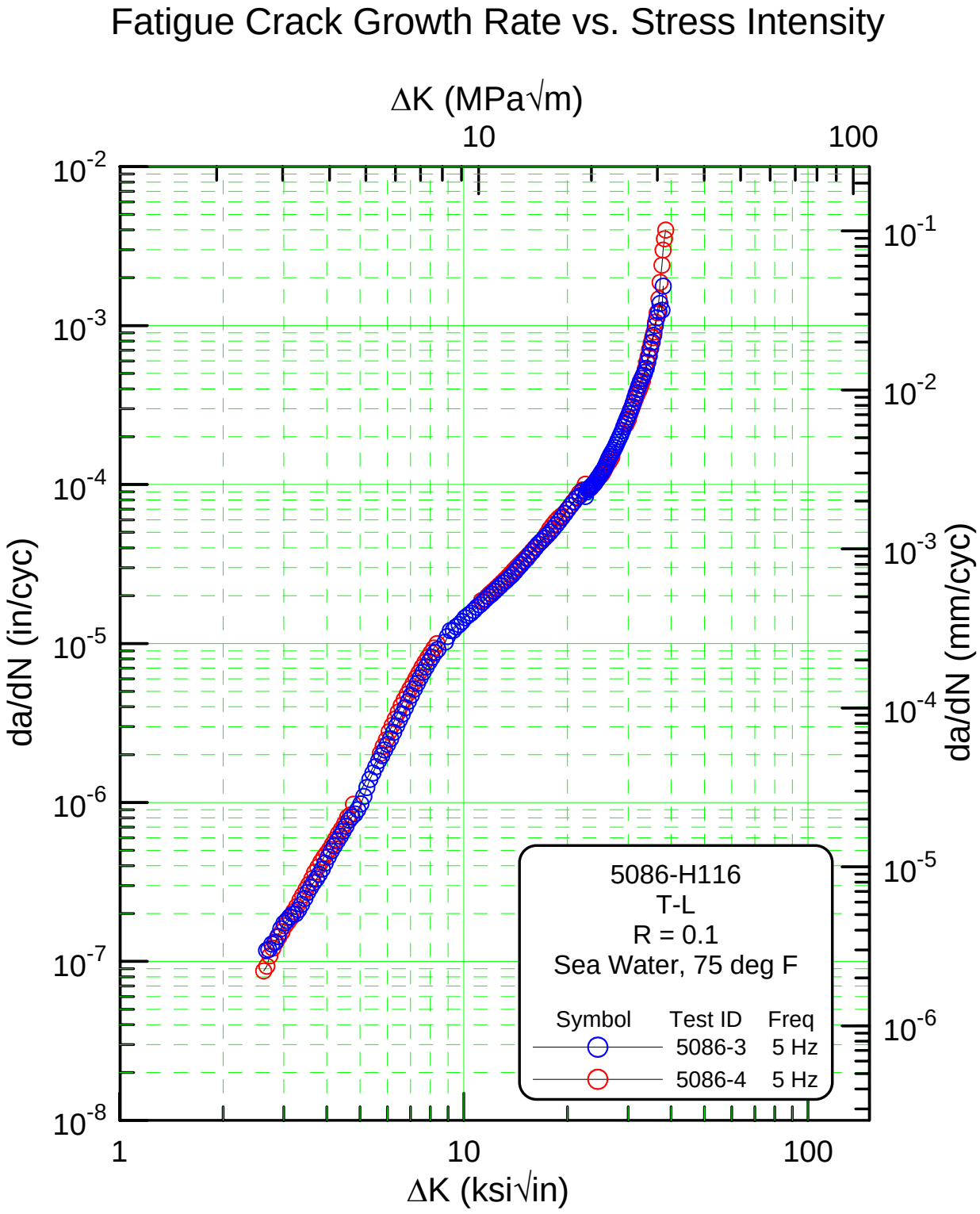

FIGURE 2.5.5: FCGR response comparing duplicate tests for the 5086-H116 alloy in seawater.

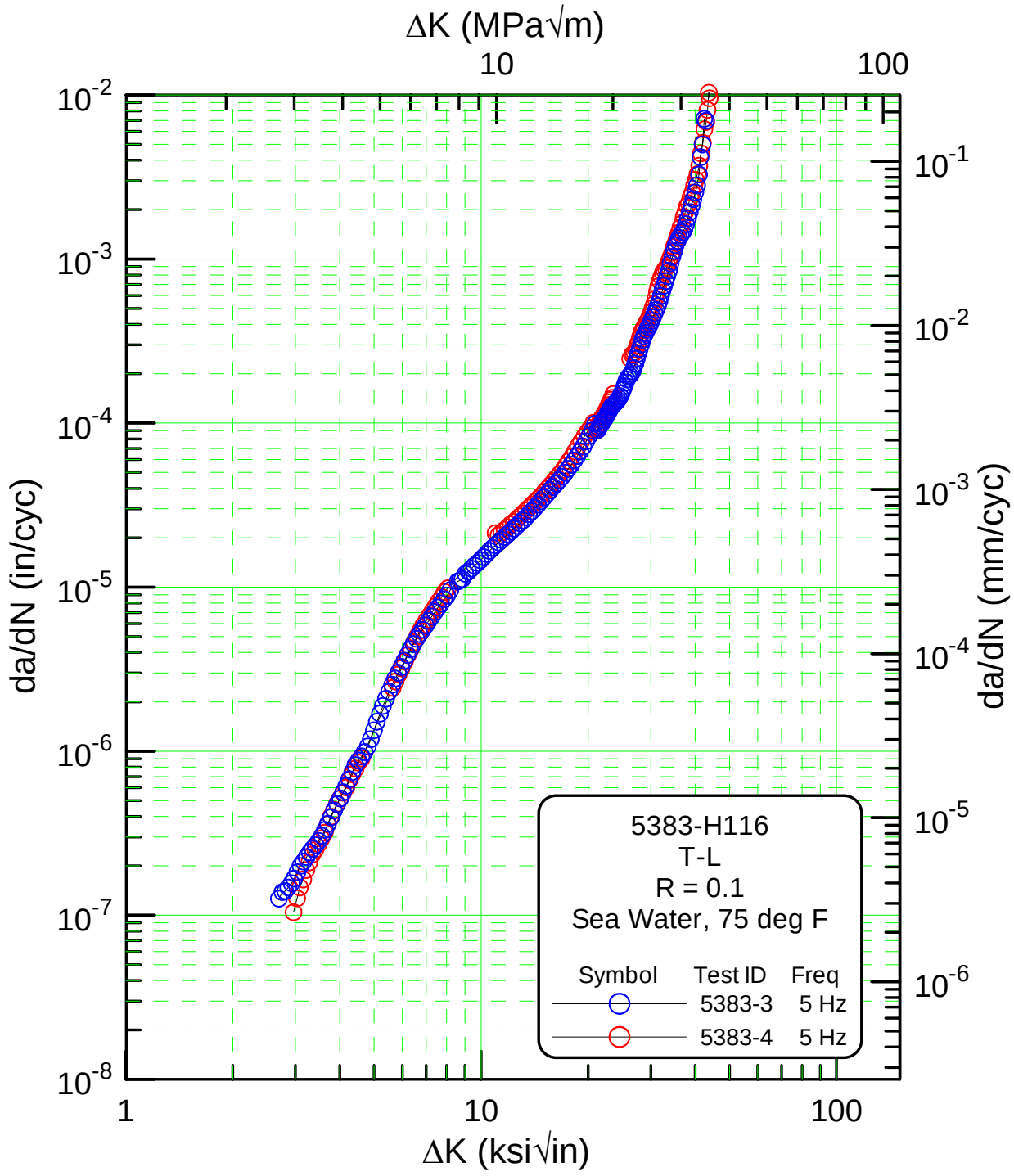

FIGURE 2.5.6: FCGR response comparing duplicate tests for the 5383-H116 alloy in seawater.

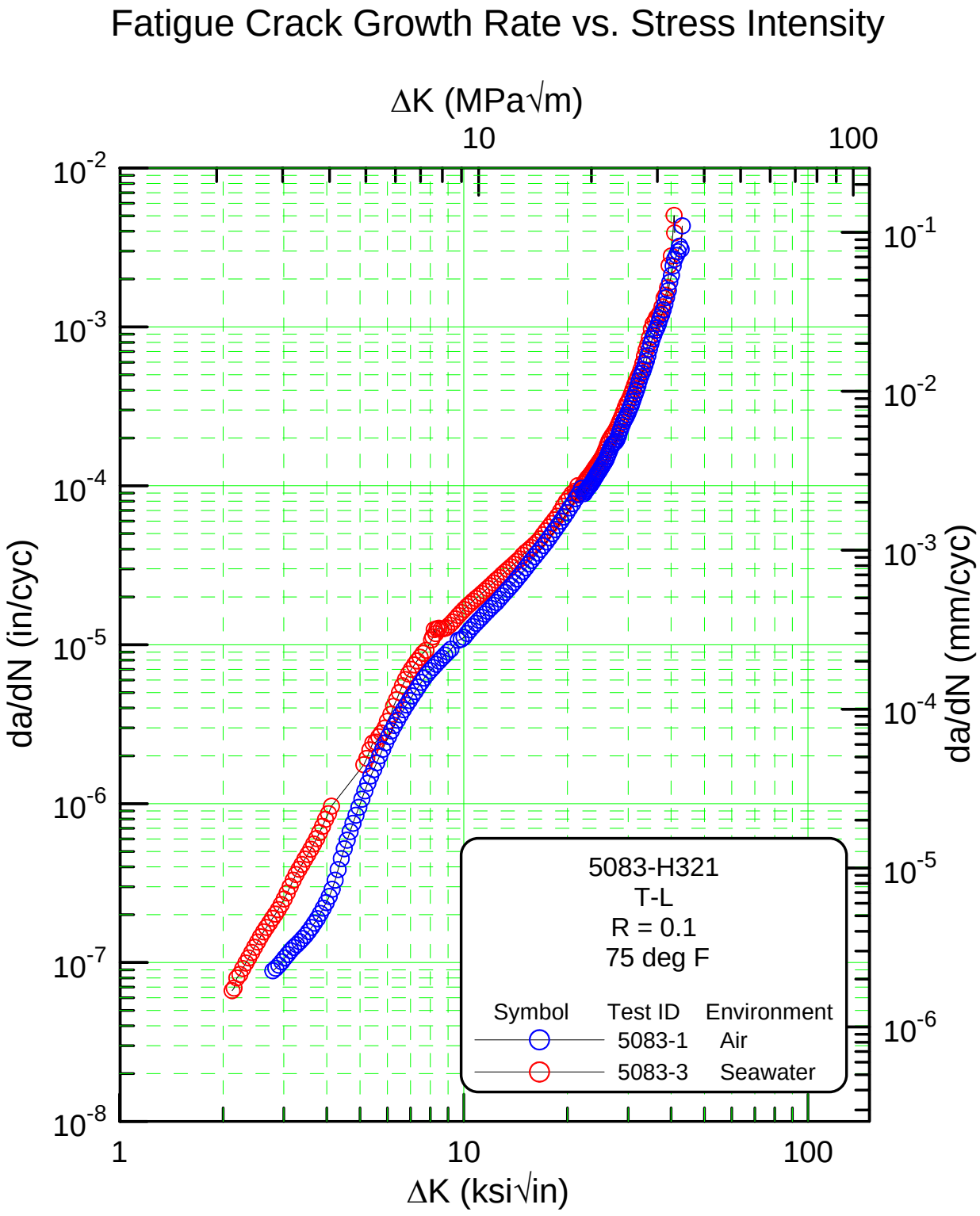

FIGURE 2.5.7: FCGR response showing the effect of environment for the 5083-H321 alloy.

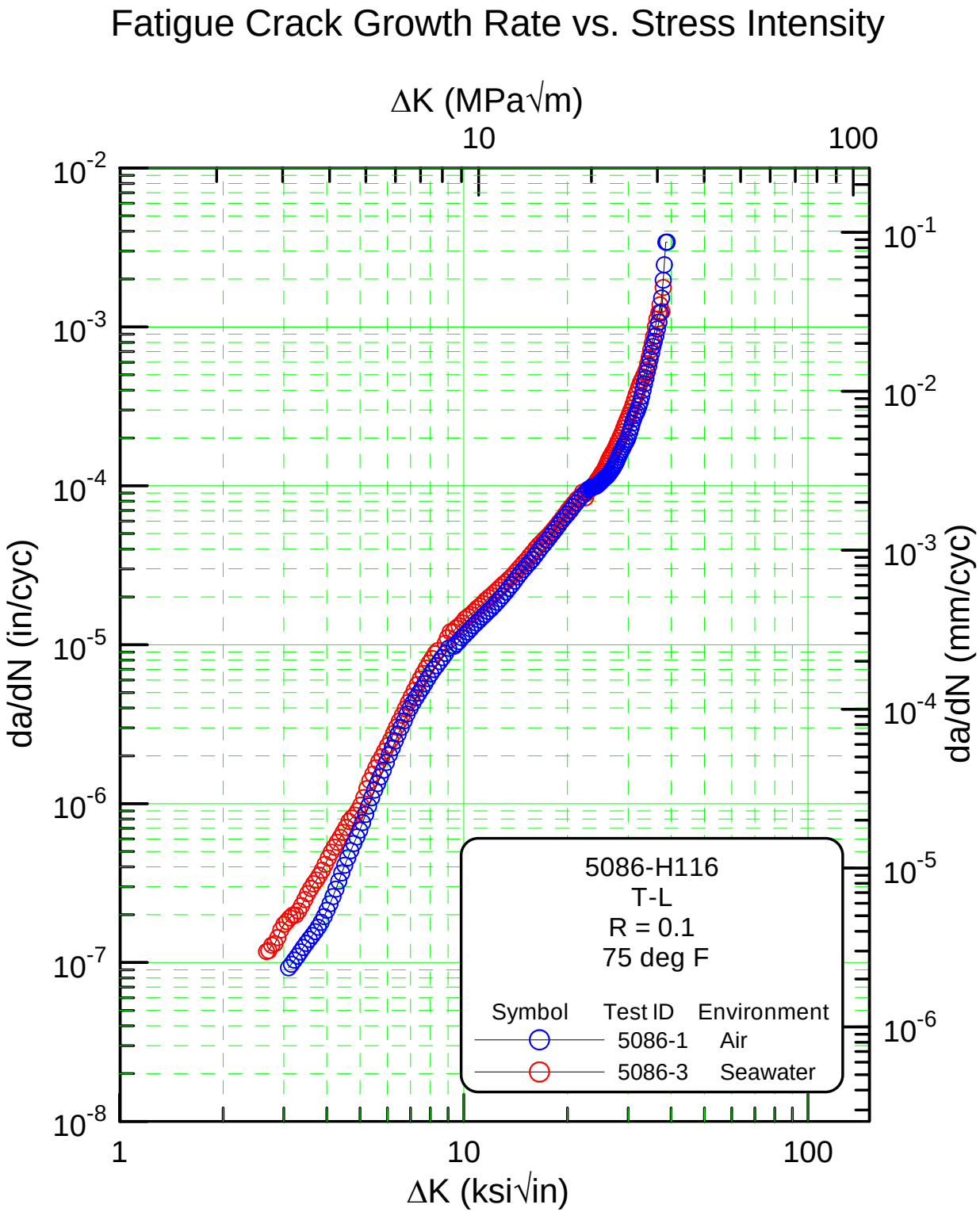

FIGURE 2.5.8: FCGR response showing the effect of environment for the 5086-H116 alloy.

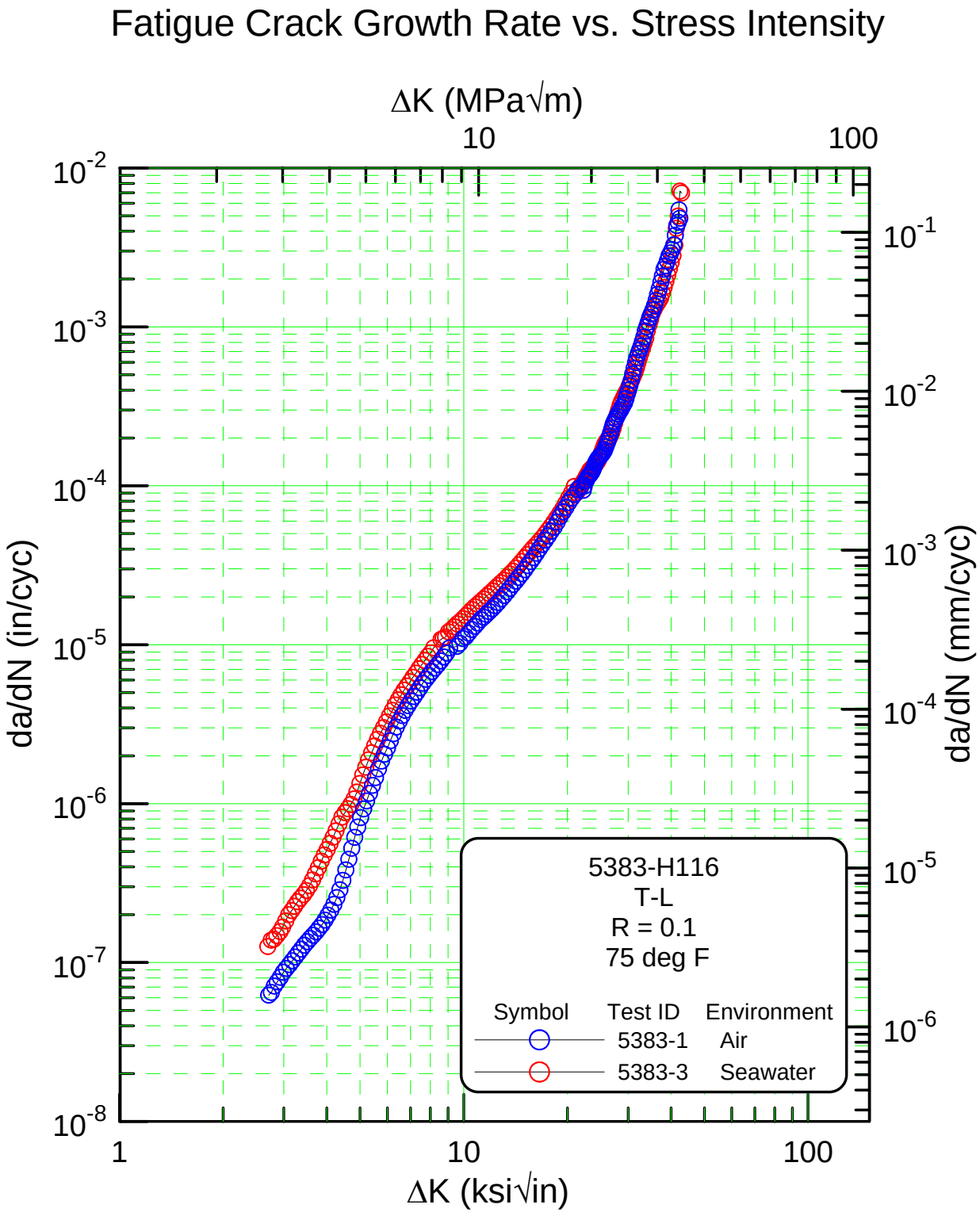

FIGURE 2.5.9: FCGR response showing the effect of environment for the 5383-H116 alloy.

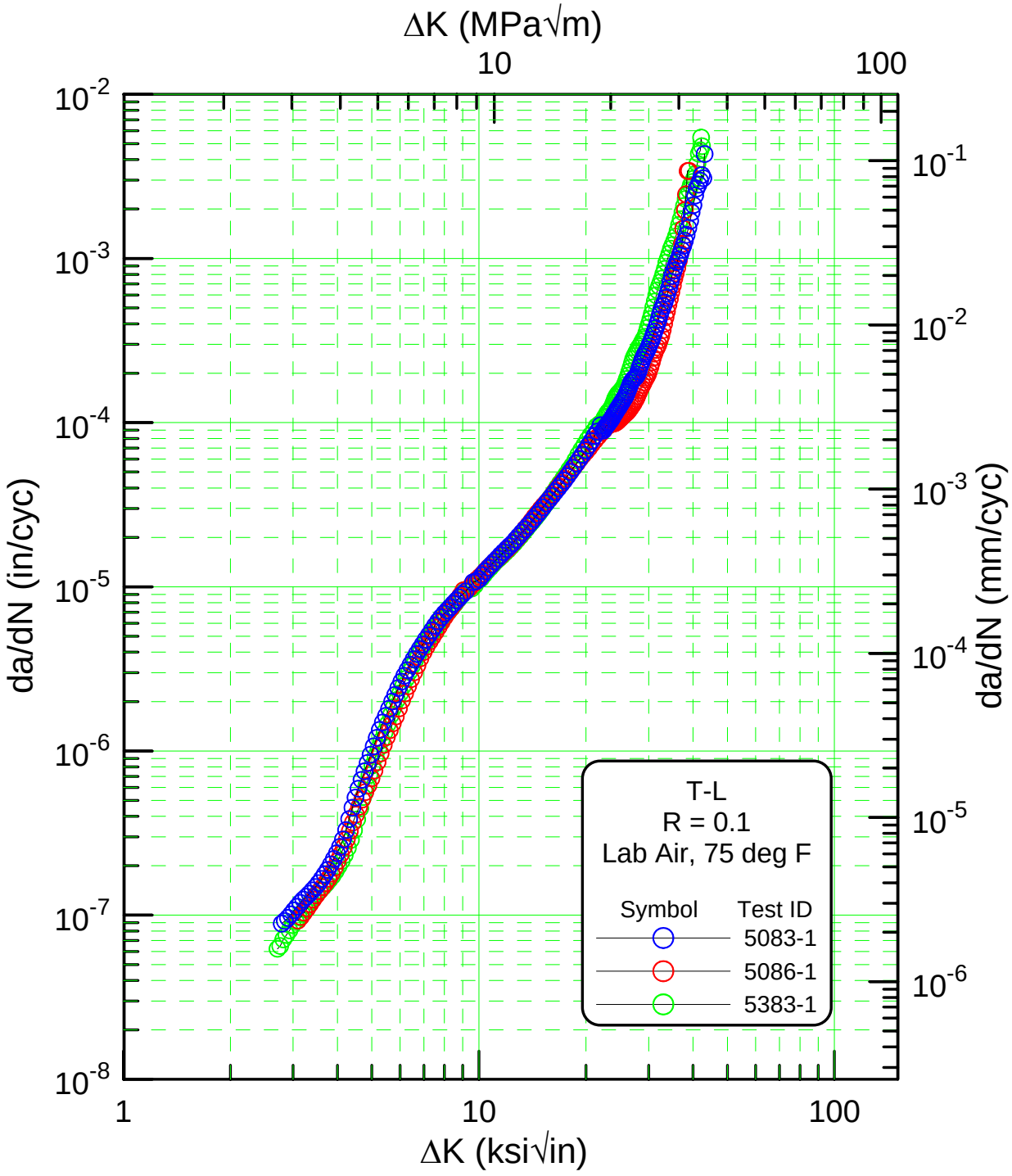

FIGURE 2.5.10: FCGR response showing the effect of the grade of material in laboratory air.

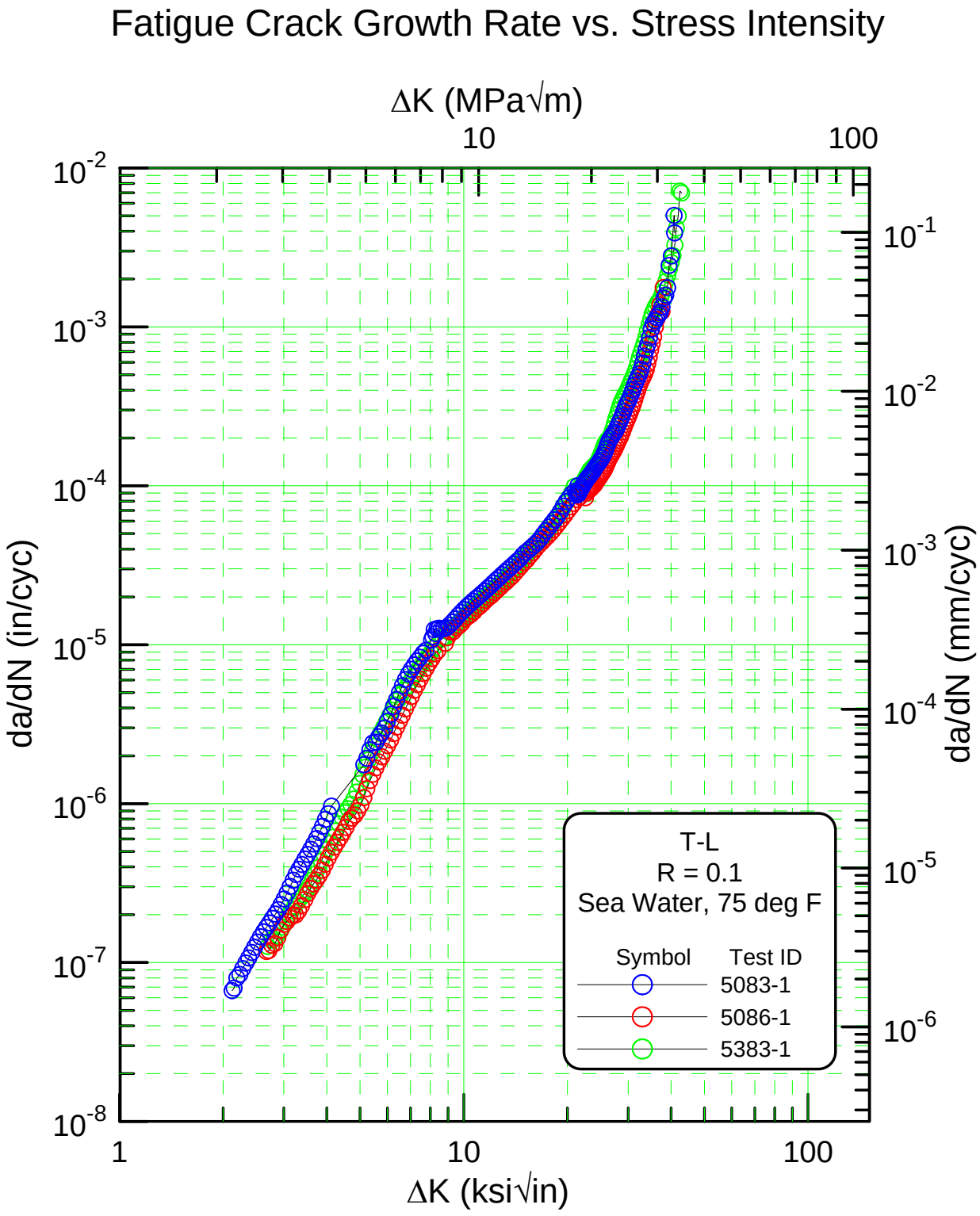

FIGURE 2.5.11: FCGR response showing the effect of the grade of material in seawater.

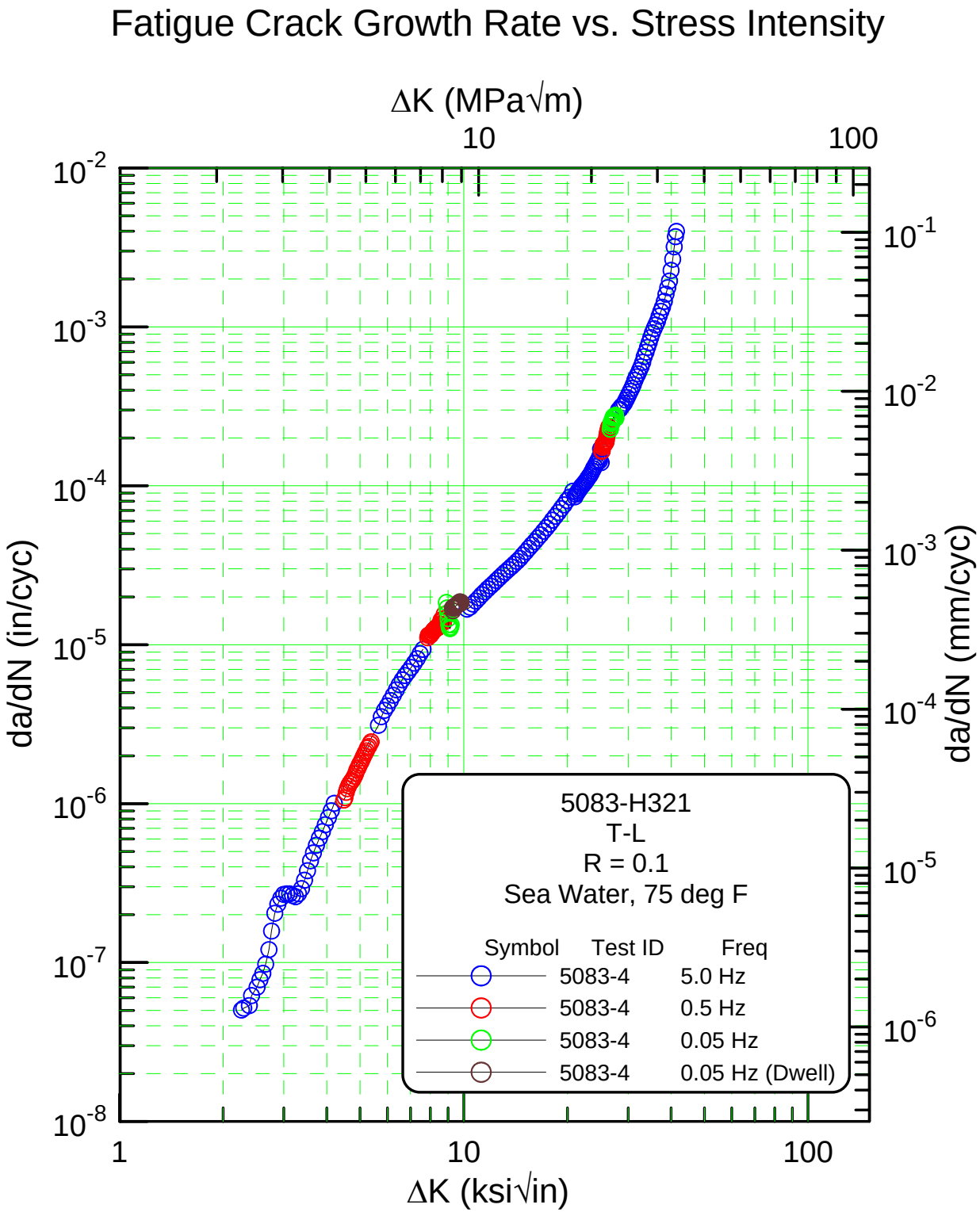

FIGURE 2.5.12: FCGR response showing the effect of frequency for the 5083-H321 alloy in seawater.

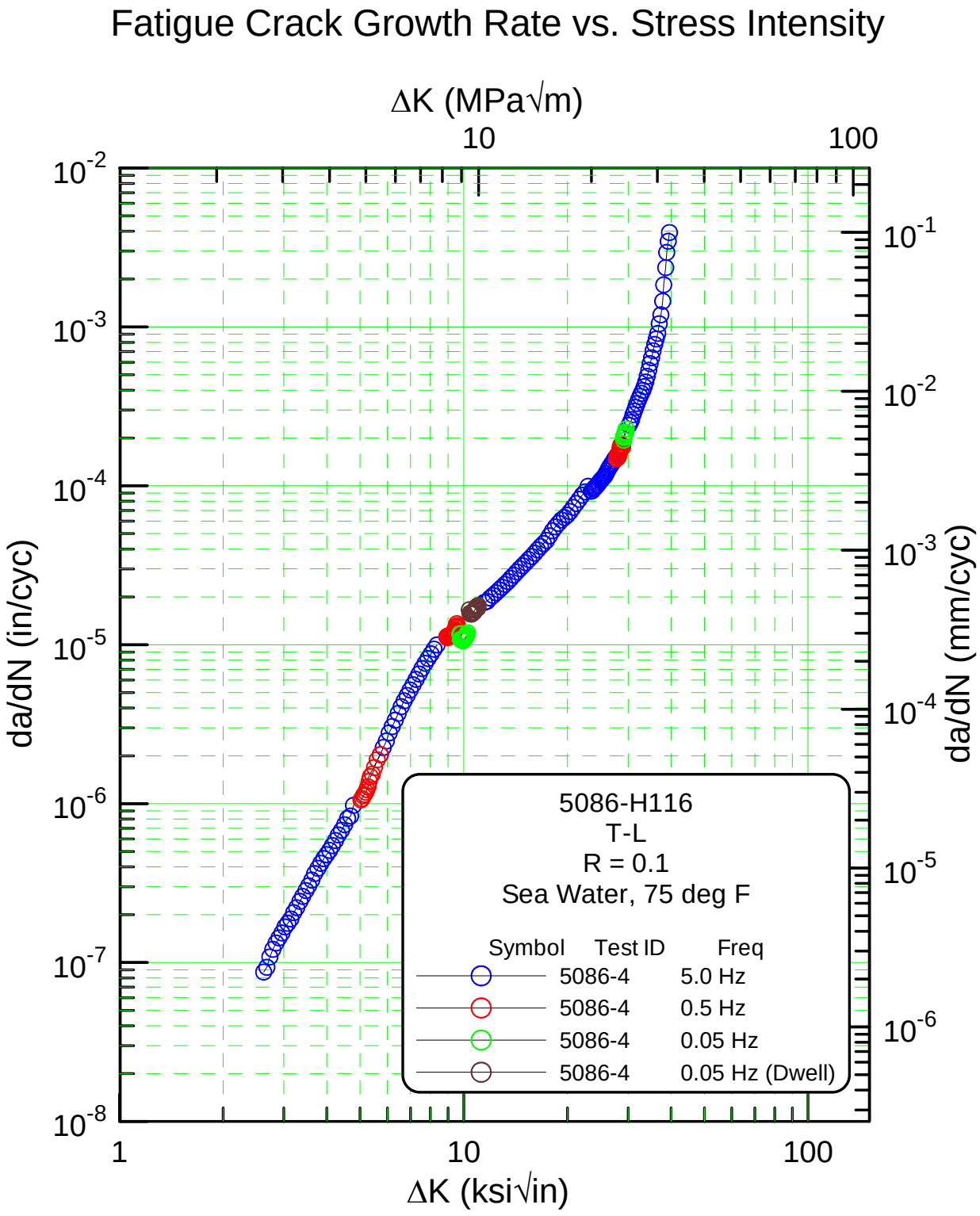

FIGURE 2.5.13: FCGR response showing the effect of frequency for the 5086-H116 alloy in seawater.

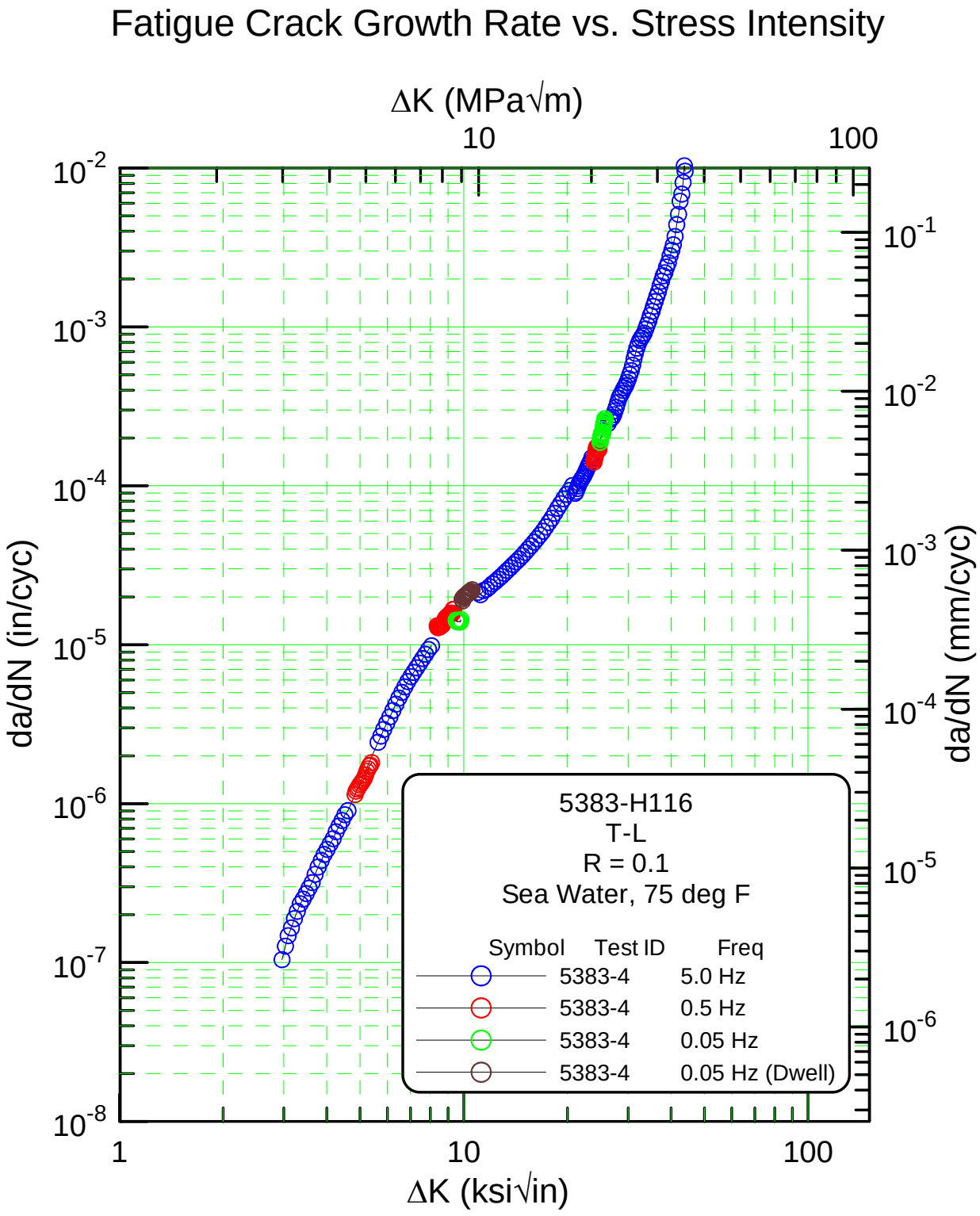

FIGURE 2.5.14: FCGR response showing the effect of frequency for the 5383-H116 alloy in seawater.

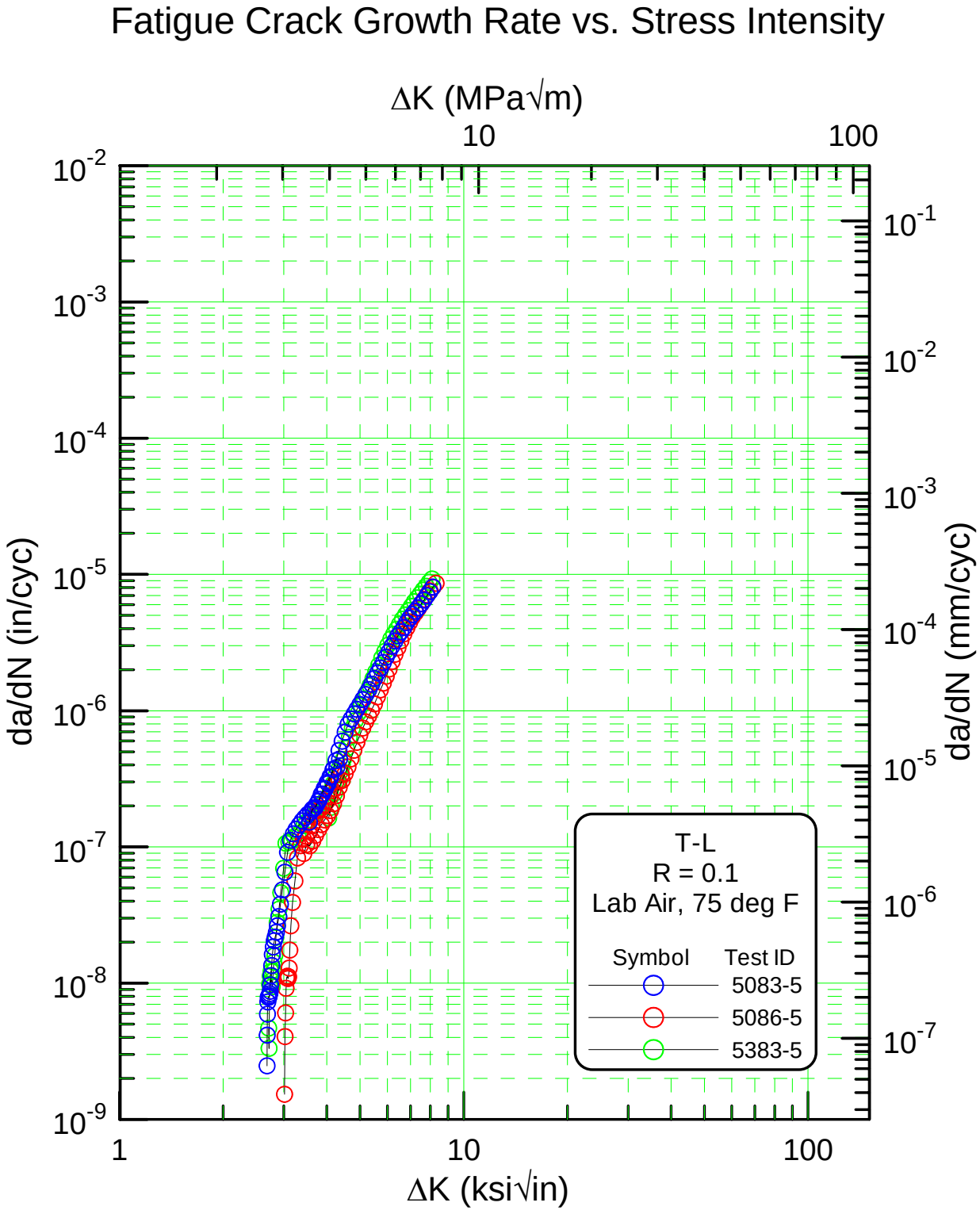

FIGURE 2.5.15: FCGR response showing the effect of the alloy on near-threshold behavior.

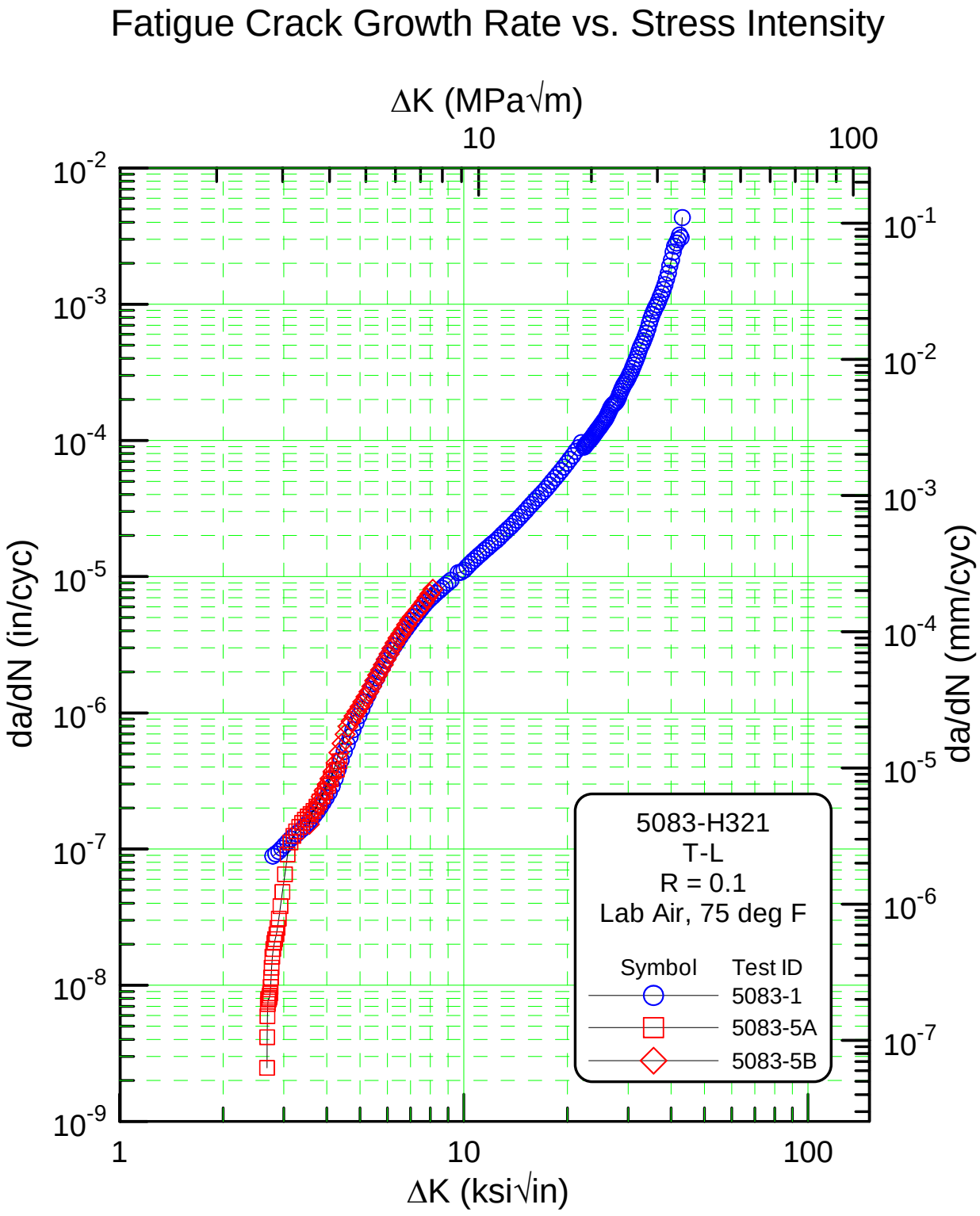

FIGURE 2.5.16: FCGR response comparing near-threshold behavior with previous increasing K data for the 5083-H321 alloy. Note departure in behavior at ~1 x 10^{-7} inch/cycle.

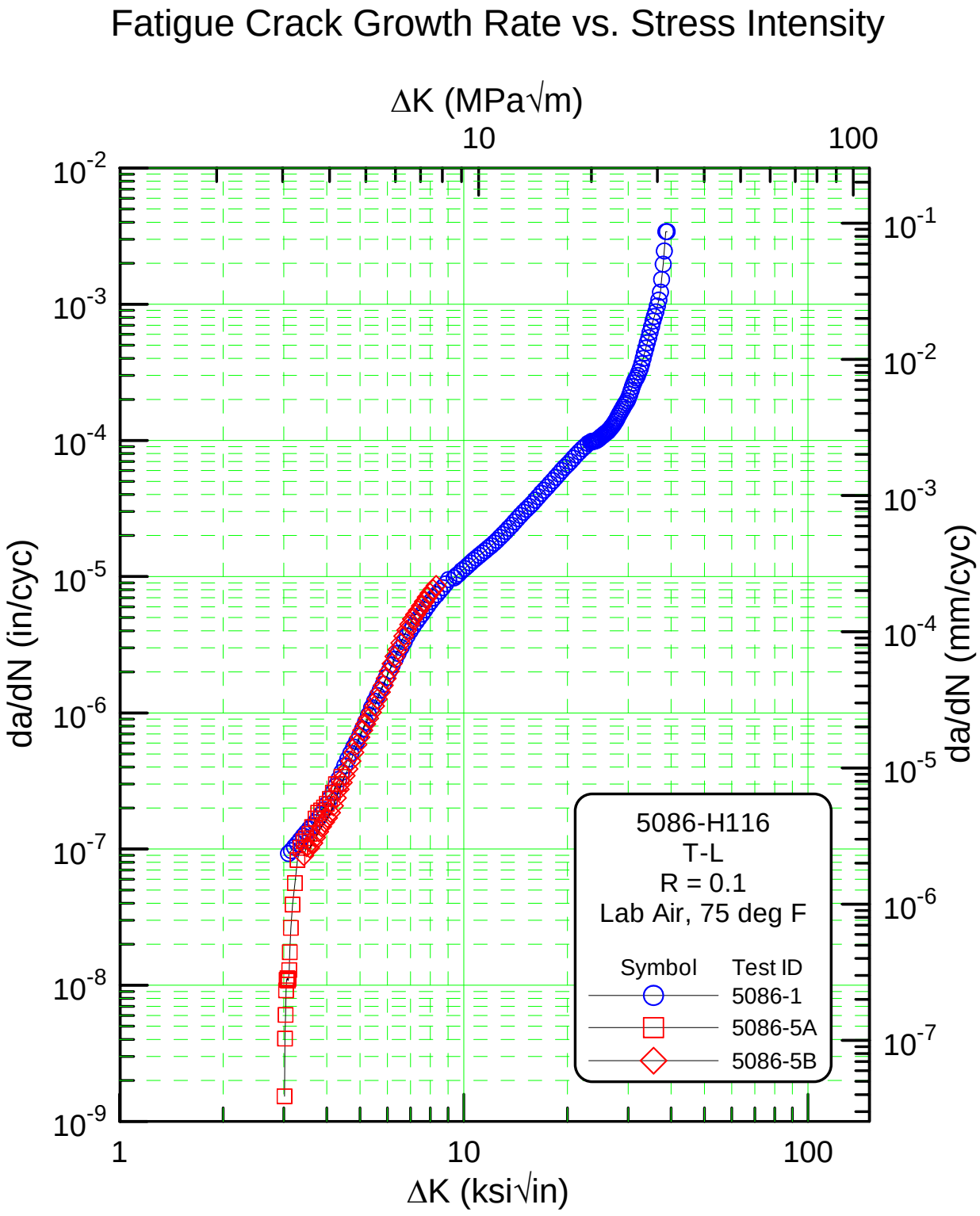

FIGURE 2.5.17: FCGR response comparing near-threshold behavior with previous increasing K data for the 5086-H116 alloy. Note departure in behavior at ~1 x 10^{-7} inch/cycle.

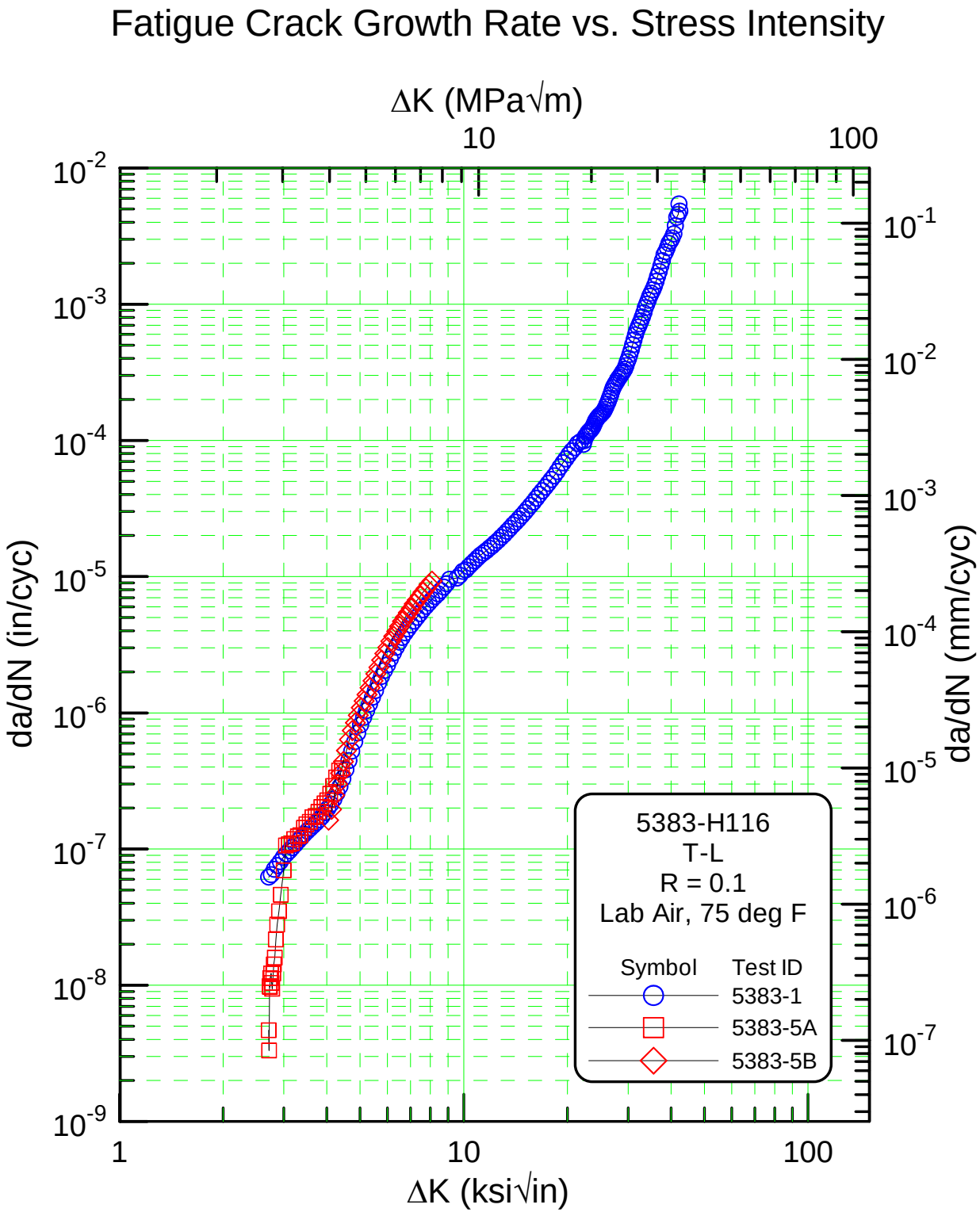

FIGURE 2.5.18: FCGR response comparing near-threshold behavior with previous increasing K data for the 5383-H116 alloy. Note departure in behavior at ~1 x 10^{-7} inch/cycle.

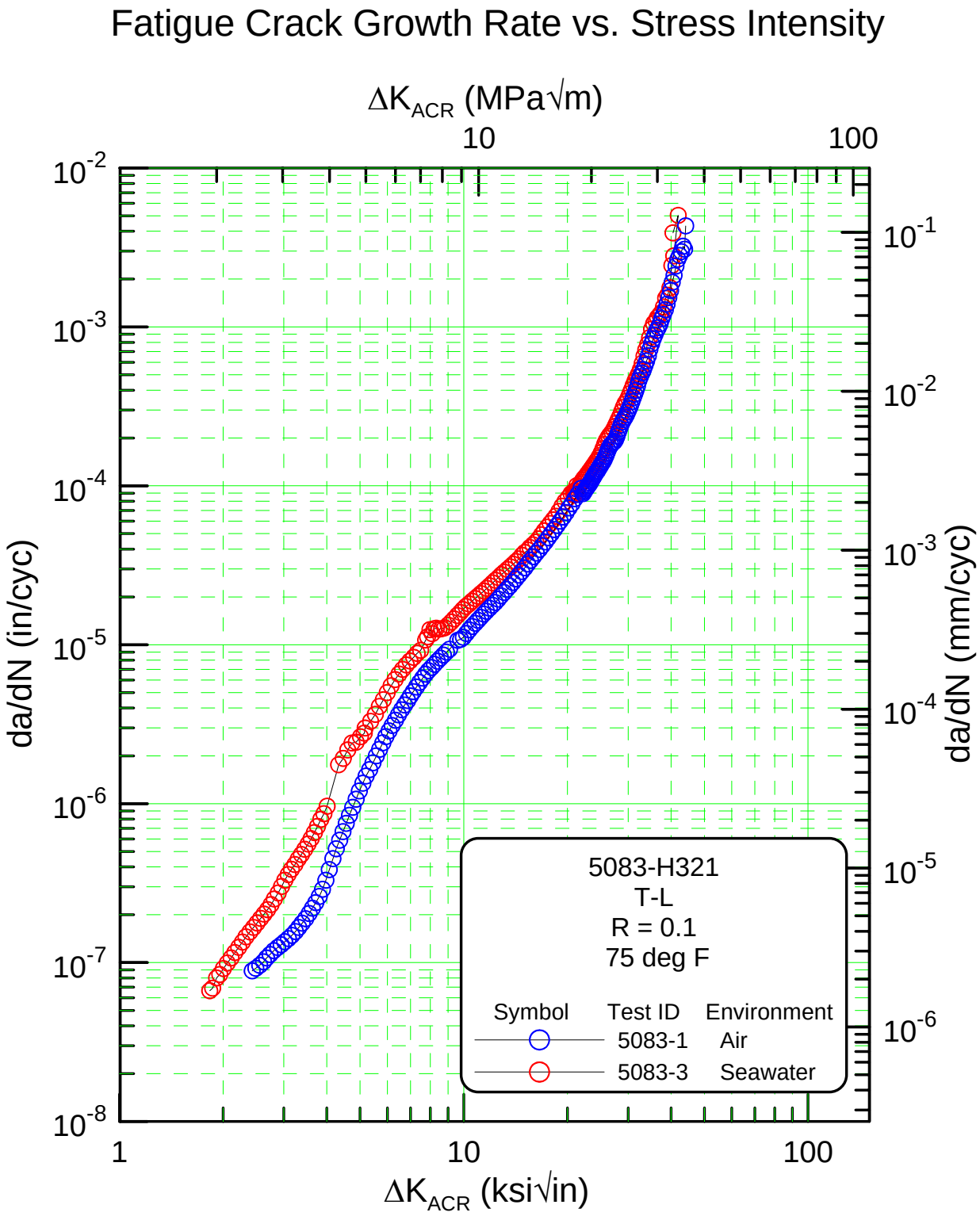

FIGURE 2.5.19: FCGR response showing the effect of environment for the 5083-H321 alloy. Data are corrected for closure using the ACR method.

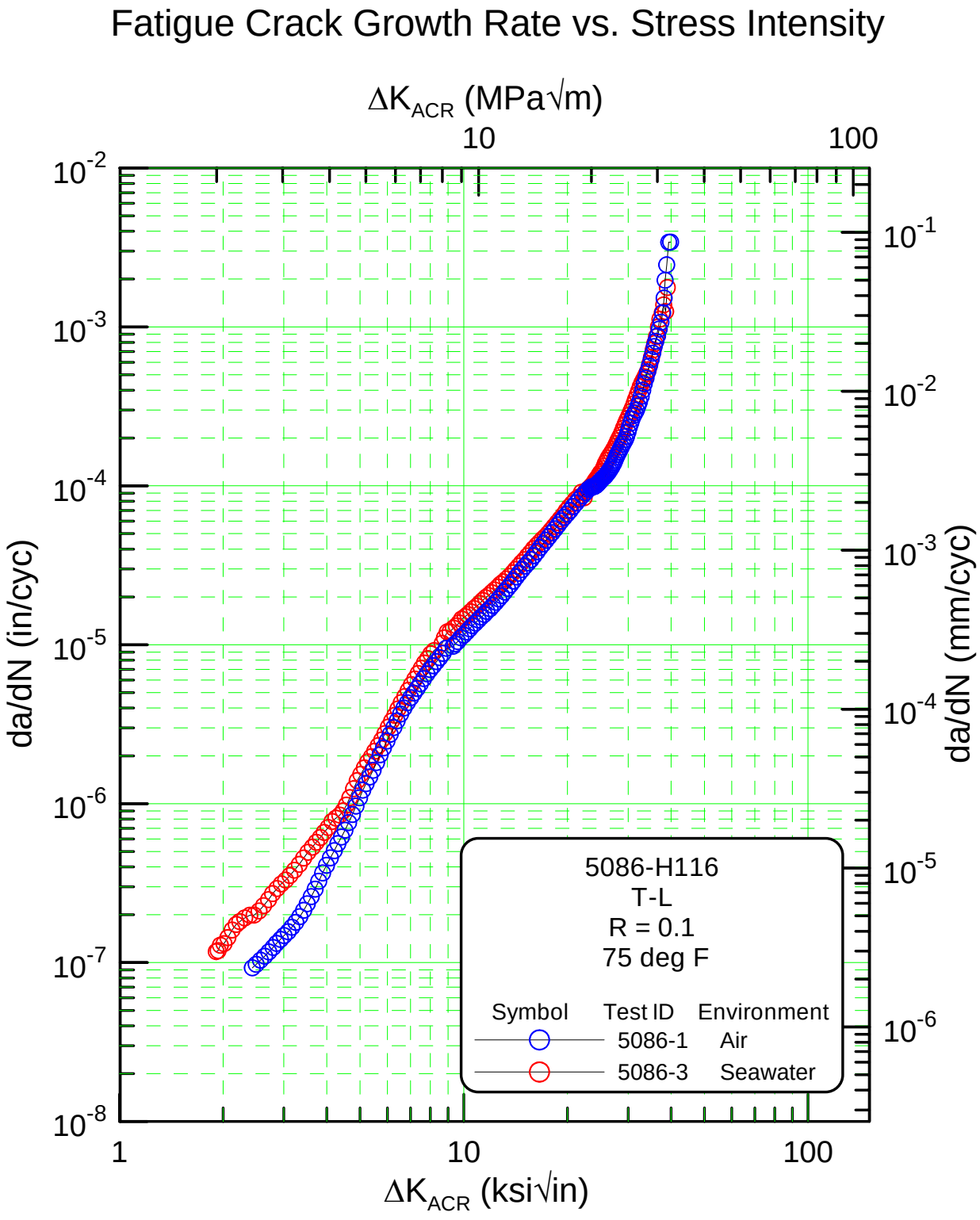

FIGURE 2.5.20: FCGR response showing the effect of environment for the 5086-H116 alloy. Data are corrected for closure using the ACR method.

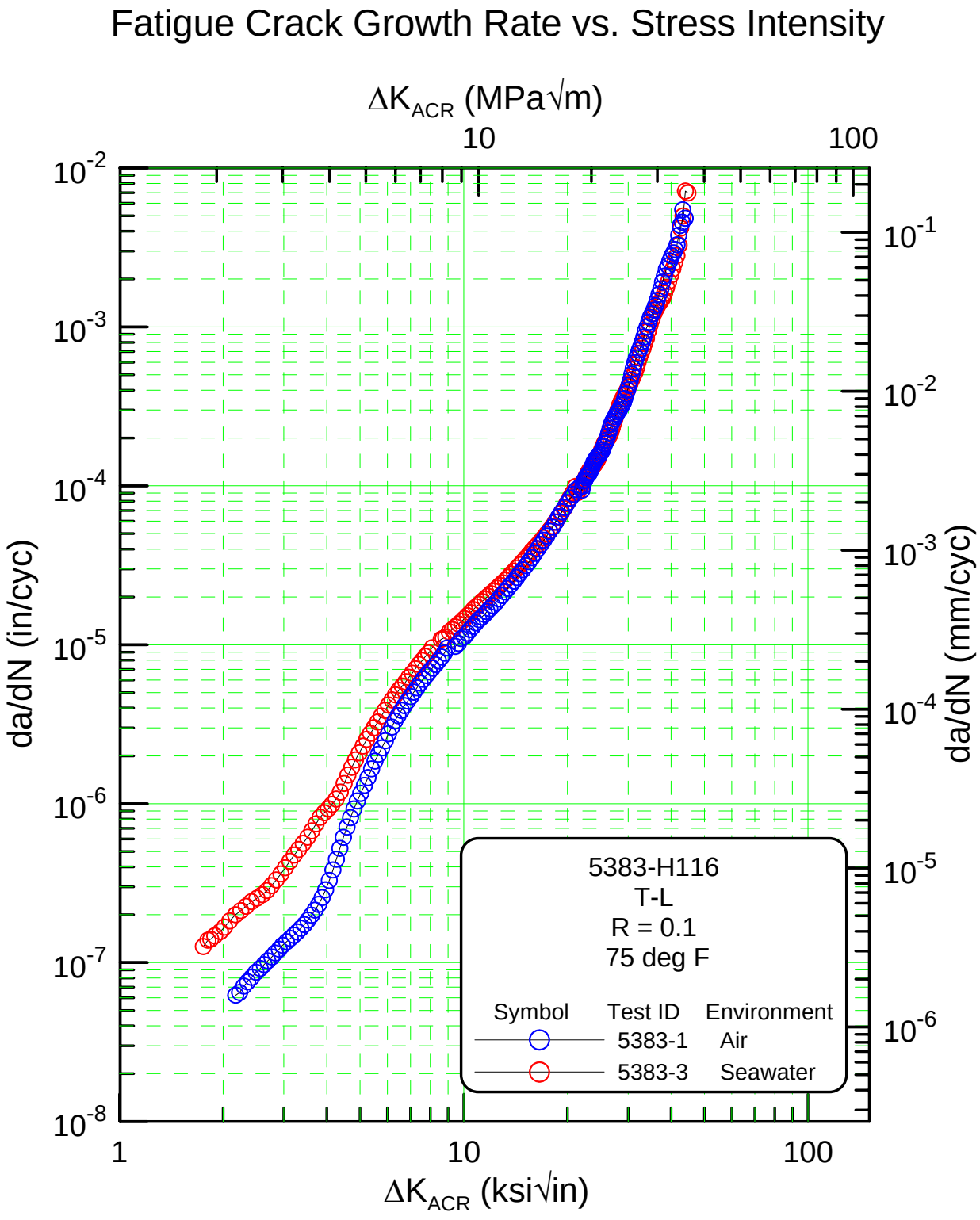

FIGURE 2.5.21: FCGR response showing the effect of environment for the 5383-H116 alloy. Data are corrected for closure using the ACR method.

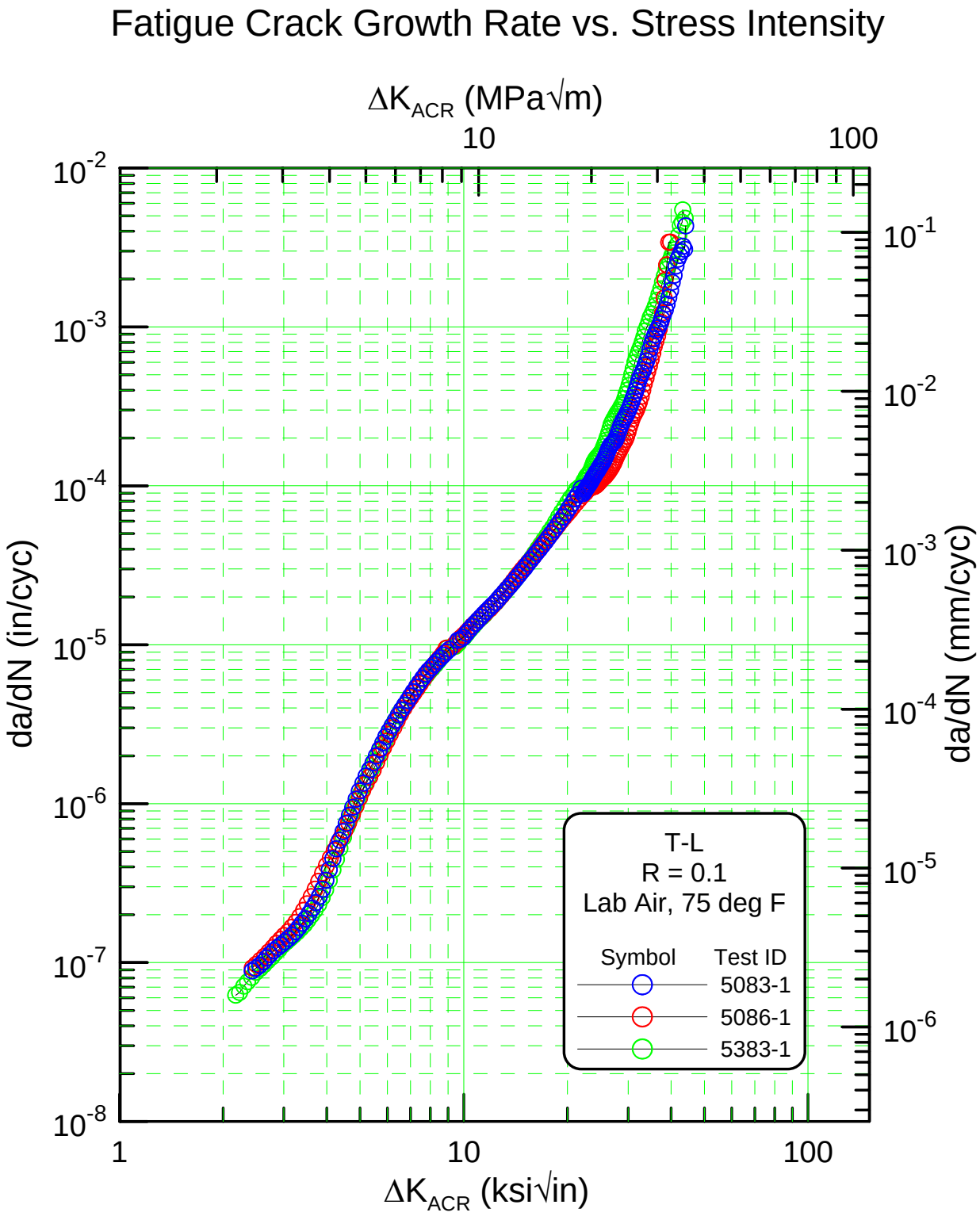

FIGURE 2.5.22: FCGR response showing the effect of the grade of material in laboratory air. Data are corrected for closure using the ACR method.

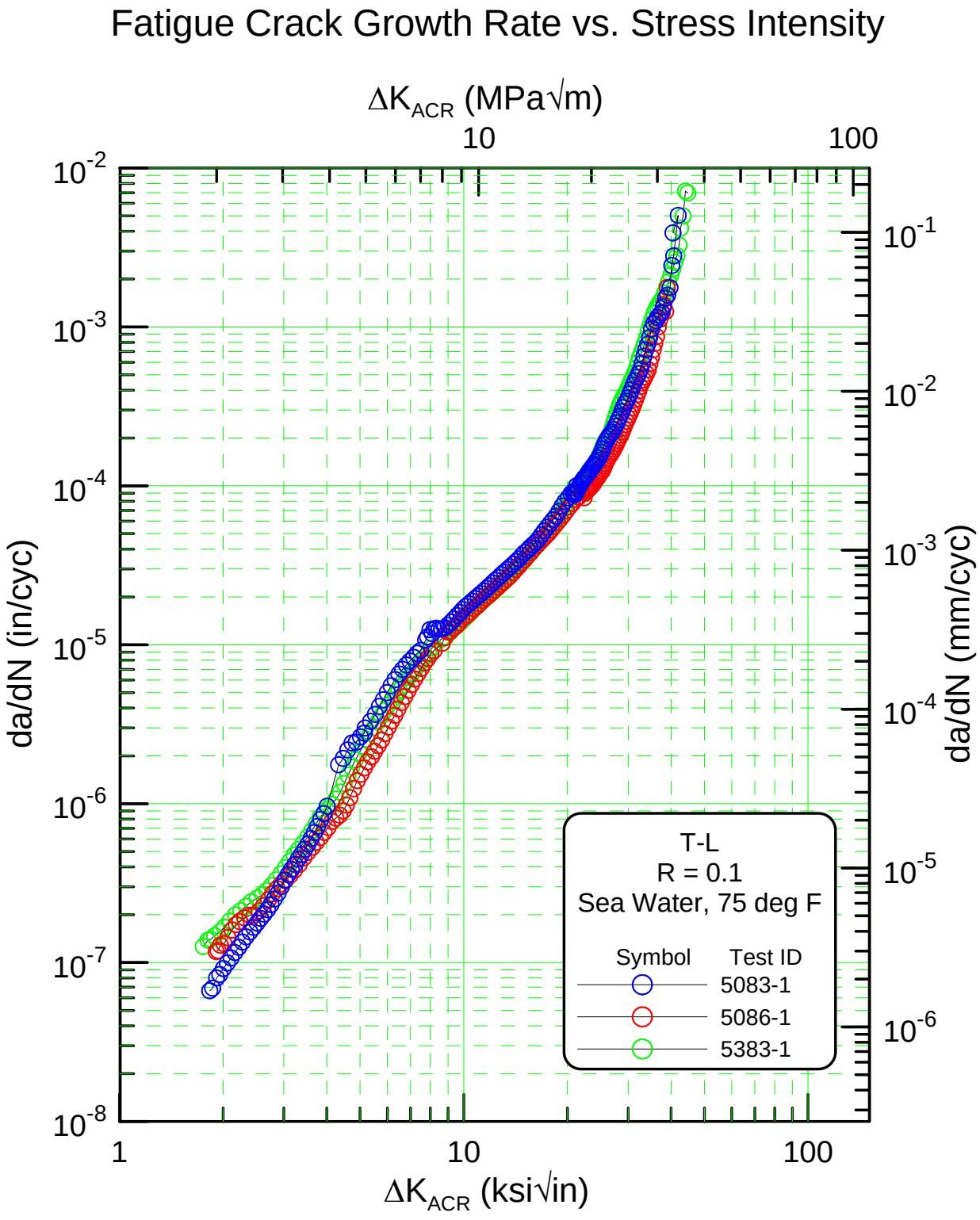

FIGURE 2.5.23: FCGR response showing the effect of the grade of material in seawater. Data are corrected for closure using the ACR method.

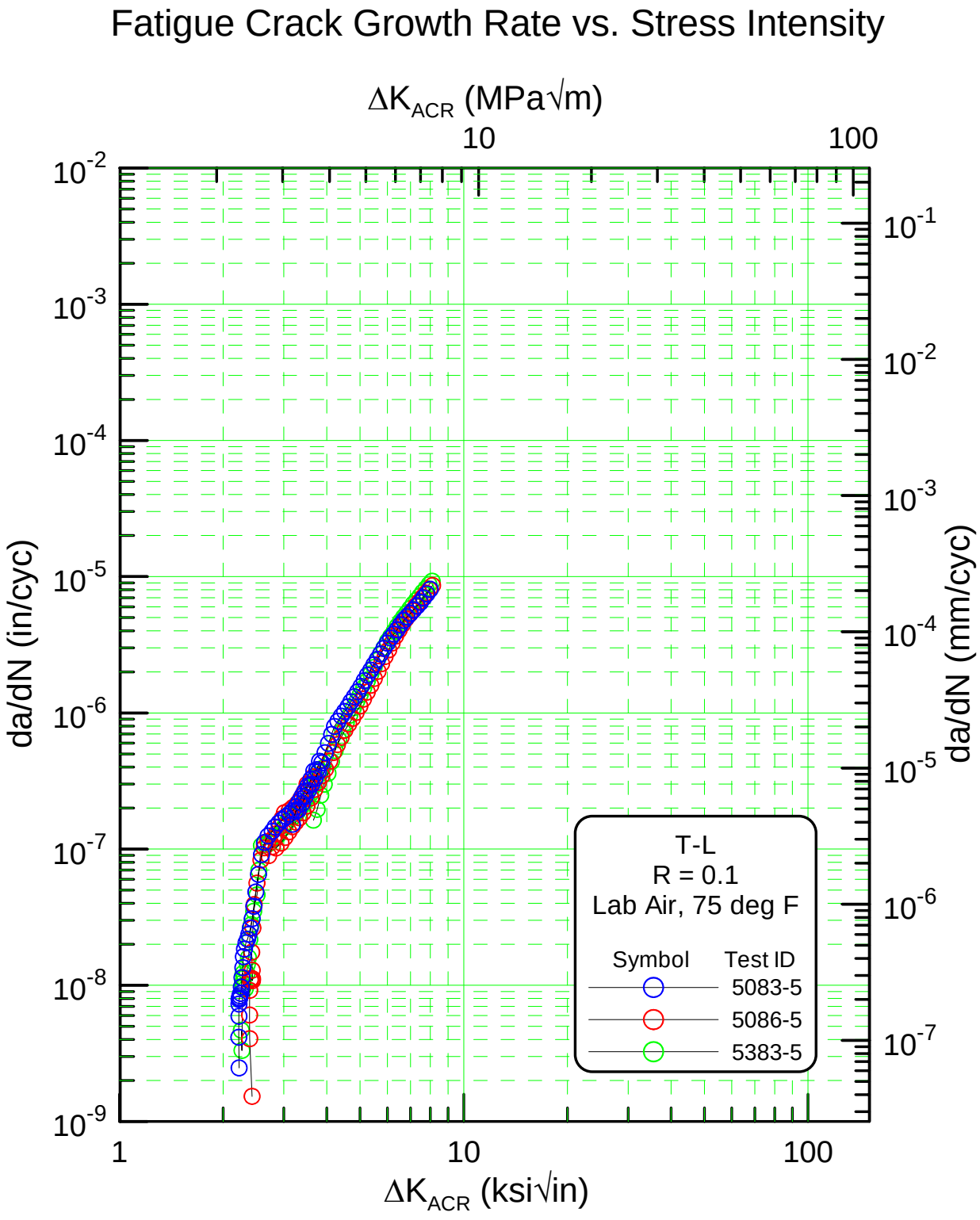

FIGURE 2.5.24: FCGR response showing the effect of the alloy on near-threshold behavior. Data are corrected for closure using the ACR method.

3.0 Non-Linear Fracture Toughness Characterization

3.1 Introduction

Non-Linear fracture toughness testing (NLFT) testing was conducted on three grades of aluminum alloys designated 5083-H321, 5086-H116 and 5383-H116. A compact tension sample having a width of 2.000 inches and a thickness of 0.500 inches was chosen for the majority of the NLFT testing. In addition, a compact tension sample having a width of 4.000 inches and a thickness of 0.500 inches was used to evaluate size effects. For each grade of material, two replicate tests were conducted using full thickness samples without side grooves. A third set of samples was tested with side-grooves to evaluate constraint effects. All samples were machined in the T-L orientation and all samples were tested laboratory air. Testing was performed in accordance with the ASTM E 1820-01 "Standard Test Method for Measurement of Fracture Toughness. A single specimen unloading compliance technique was used to monitor stable crack extension.

3.2 Test Equipment

The tests were conducted on one MTS load frame equipped with a 5,000 lbf load cell and interfaced to an Adwin-Gold FTA computer system and configured for fracture toughness testing. An MTS model 632.03B-30 (opt 006) clip gage was used for load-line displacement measurement. Compliance measurement accuracy was enhanced by mounting needle bearings in both the clevis holes and the specimen holes to minimize non-linearity in the load-displacement signal due to pin friction. Laboratory temperature and relative humidity were controlled to 75°F +/- 2°F and 40% +/- 5% R.H. throughout the entire period of testing.

3.3 Sample Preparation

The test samples were machined according to Figure 3.3.1.

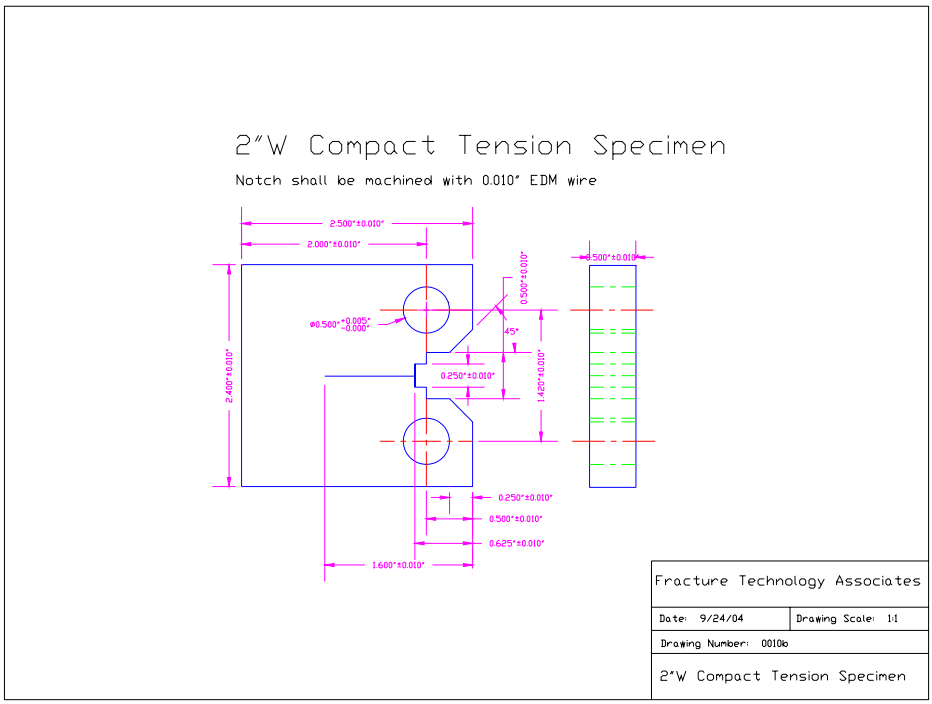

FIGURE 3.3.1: Diagram of C(T) sample for fracture toughness testing
(diagram reproduction not to scale)

3.4 Test Procedure

Data storage (.raw file extension) was set to 2 points per second for load displacement data in the ramp up/ramp down mode; 0.2 points per second for load displacement data during the hold mode, and 10 points per second for unloading slope data (.unl file extension). The actuator loading and unloading rate was set to 0.020 inches/minute. Each test was initially ramped to the approximate precrack load and several unloading slopes were performed with a loading/unloading data acquisition rate of 10 points/second to ensure the specimens were properly seated. The correlation coefficient of each unloading slope was typically 0.99998. After verification that the unloading slopes were repeatable and that the compliance measured crack length was within 2% of the predicted crack length, actual testing commenced. Load and clip gage displacement were recorded in the analysis file every 0.0010 - 0.0020 inches of clip gage displacement or every 200 lbs. increase in load. In addition, the largest observed load and corresponding displacement were stored.

Each test was terminated after about 0.2 inches of stable crack extension. The sample was then fatigue loaded to mark the final crack extension. A nine point average of the precrack as well as the final stable crack extension was recorded and used to verify the compliance calculated crack extension.

3.5 Test Results and Discussion

Table 3.5.1 summarizes key test conditions and results. The fracture toughness results are based on the J at initiation (J_{Ic}) according to ASTM E1820-01 as well as an equivalent K at initiation designated K_{JIc}. The toughness values at initiation for the side grooved and non-side grooved samples were almost equivalent. The larger sample size gave slightly higher values of toughness at initiation. Regardless of the size of the sample or the absence or presence of the side grooves, all samples showed the same ranking of toughness with the 5086-H116 showing the highest toughness, followed by the 5083-H321, and the 5383-H116 alloy showing the lowest toughness.

The most significant difference between the side grooved and non-side grooved samples is illustrated in Figure 3.5.1. These R-curves show stable crack extension well beyond maximum load. The samples without the side grooves are representative of the fracture toughness characteristics of the 0.5 inches plate whereas the side grooved samples are representative of much thicker material since the side grooves add additional constraint and suppress plane stress behavior. Data beyond crack initiation should be used with caution since stable crack extension behavior is highly geometry/application dependent (See appendices for details). The ranking of the alloys is also clearly indicated consistent with the previous observations regarding toughness at initiation. The reproducibility of duplicate tests is also clearly indicated.

Figure 3.5.2 illustrates the effect of sample size. In all cases, the larger sample size shows slightly higher values of toughness at a given increment of crack extension. Figures 3.5.3 and 3.5.4 show the same trends but the toughness values have been presented as equivalent values of stress intensity K instead of J.

The photographs in Appendix C clearly shows the crack straightness characteristic of each test. Appendix F contains individual J vs. Δa plots. Appendix G contains load vs. load-line displacement curves. Appendix H contains the tabular results of the ASTM 1820 analyses including a summary of validity statements for each test.

TABLE 3.5.1--*Summary of Fracture Toughness Test Conditions and Results*

Temperature: **75 deg F**
Orientation: **T-L**
Environment: **Lab Air (RH = 40%)**

Test ID	Material	Sample Size (W, in)	Side-Groove	J_{Ic}-1820 (in-lb/in^2)	K_{JIC} (ksi √in)	Comments
5083-FT-1	5083-H321	2.00	no	96.6	33.4	Significant crack tunneling
5083-FT-2	5083-H321	2.00	no	91.8	32.6	Significant crack tunneling
5083-FT-3	5083-H321	2.00	yes	111.4	35.9	Straight crack front
5083-FT-5	5083-H321	4.00	no	146.9	41.2	Significant crack tunneling
5086-FT-1	5086-H116	2.00	no	155.4	42.3	Significant crack tunneling
5086-FT-2	5086-H116	2.00	no	147.6	41.3	Significant crack tunneling
5086-FT-3	5086-H116	2.00	yes	155.2	42.3	Straight crack front
5086-FT-5	5086-H116	4.00	no	201.0	48.2	Significant crack tunneling
5383-FT-1	5383-H116	2.00	no	86.6	31.6	Significant crack tunneling
5383-FT-2	5383-H116	2.00	no	86.1	31.5	Significant crack tunneling
5383-FT-3	5383-H116	2.00	yes	90.3	32.3	Straight crack front
5383-FT-5	5383-H116	4.00	no	99.9	34.0	Significant crack tunneling

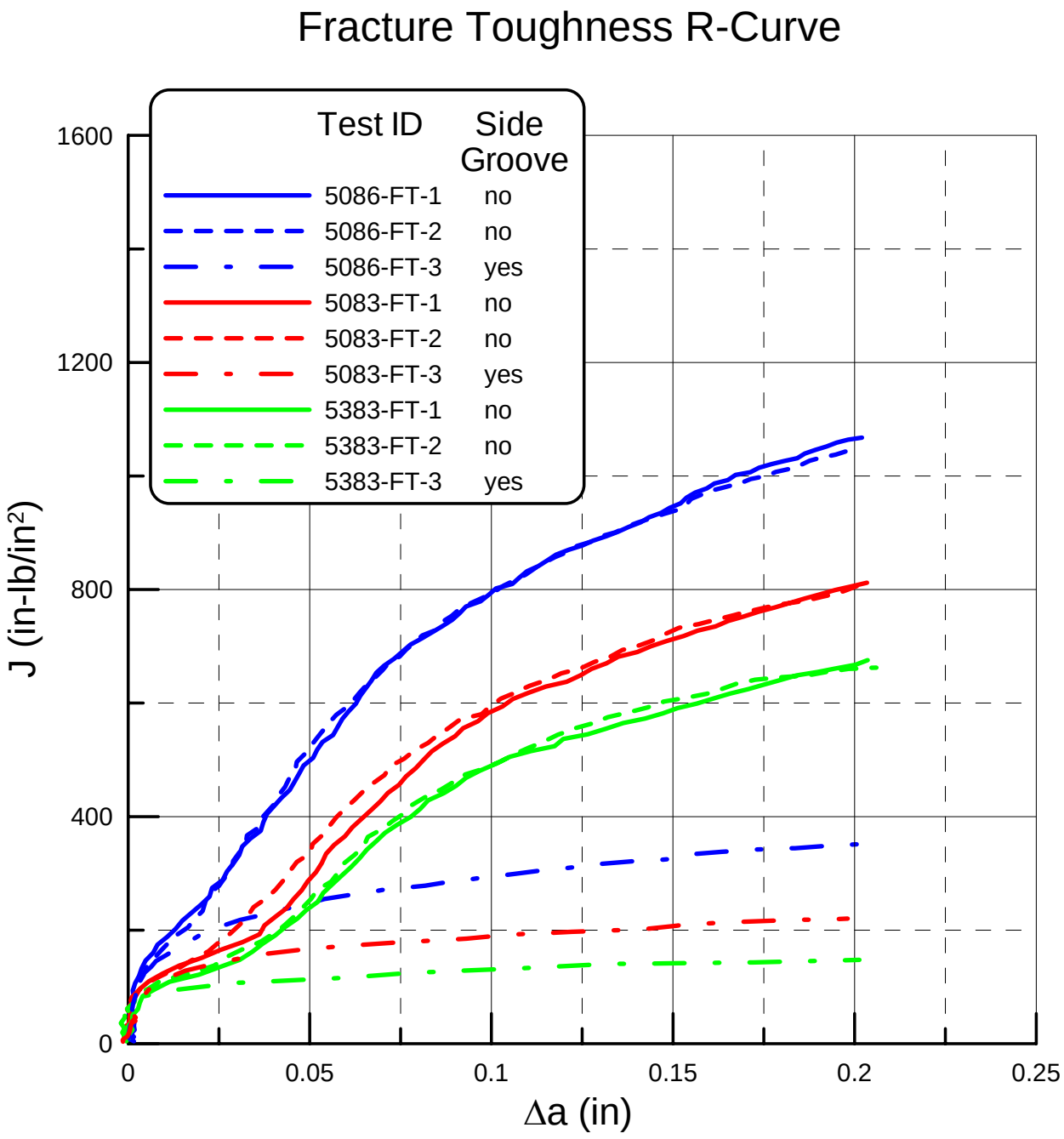

FIGURE 3.5.1: Non-linear fracture toughness showing ranking of alloys as well as duplicate test results and the effect of side grooves.

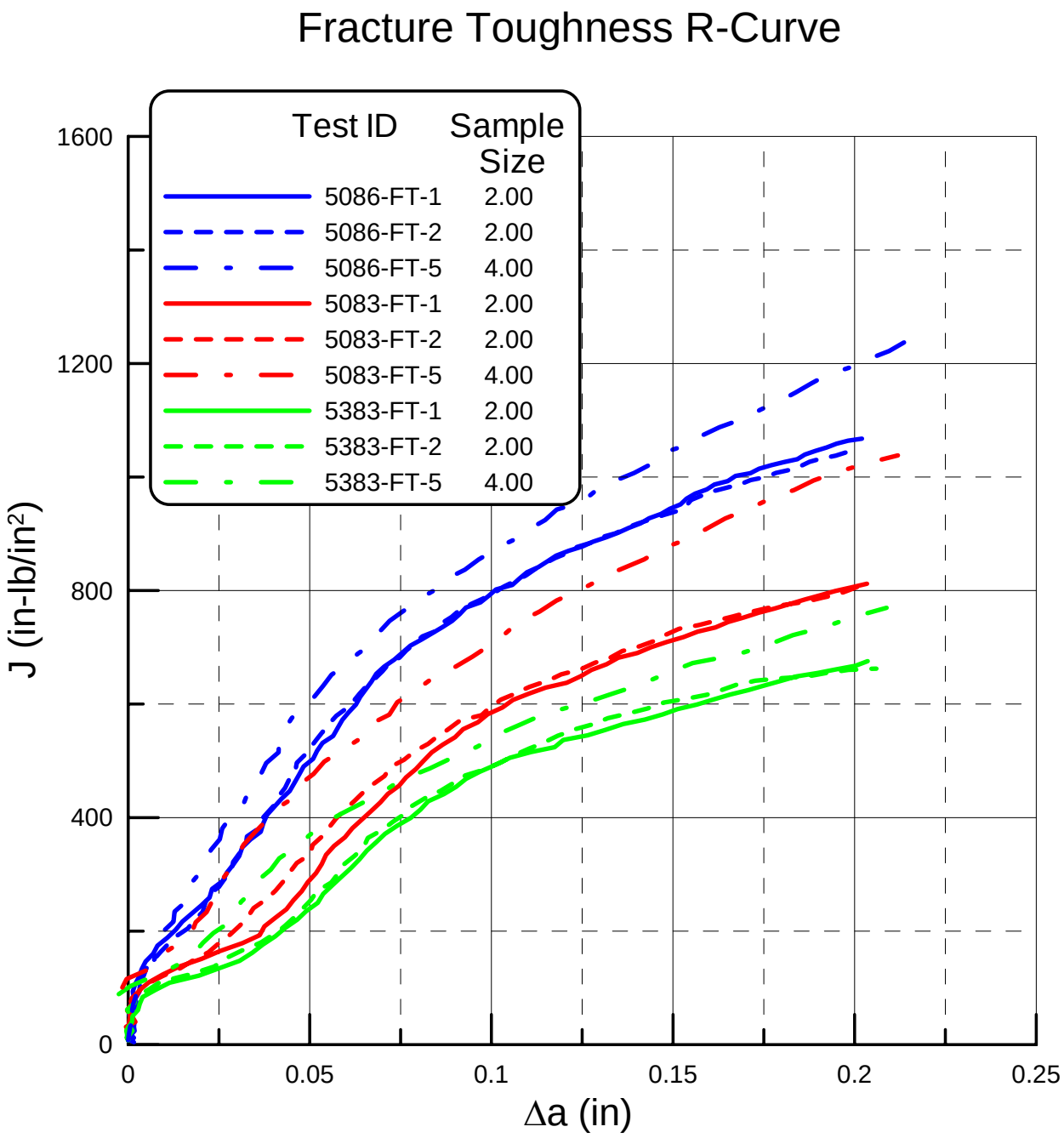

FIGURE 3.5.2: Non-linear fracture toughness showing ranking of alloys as well as duplicate test results and the effect of sample size.

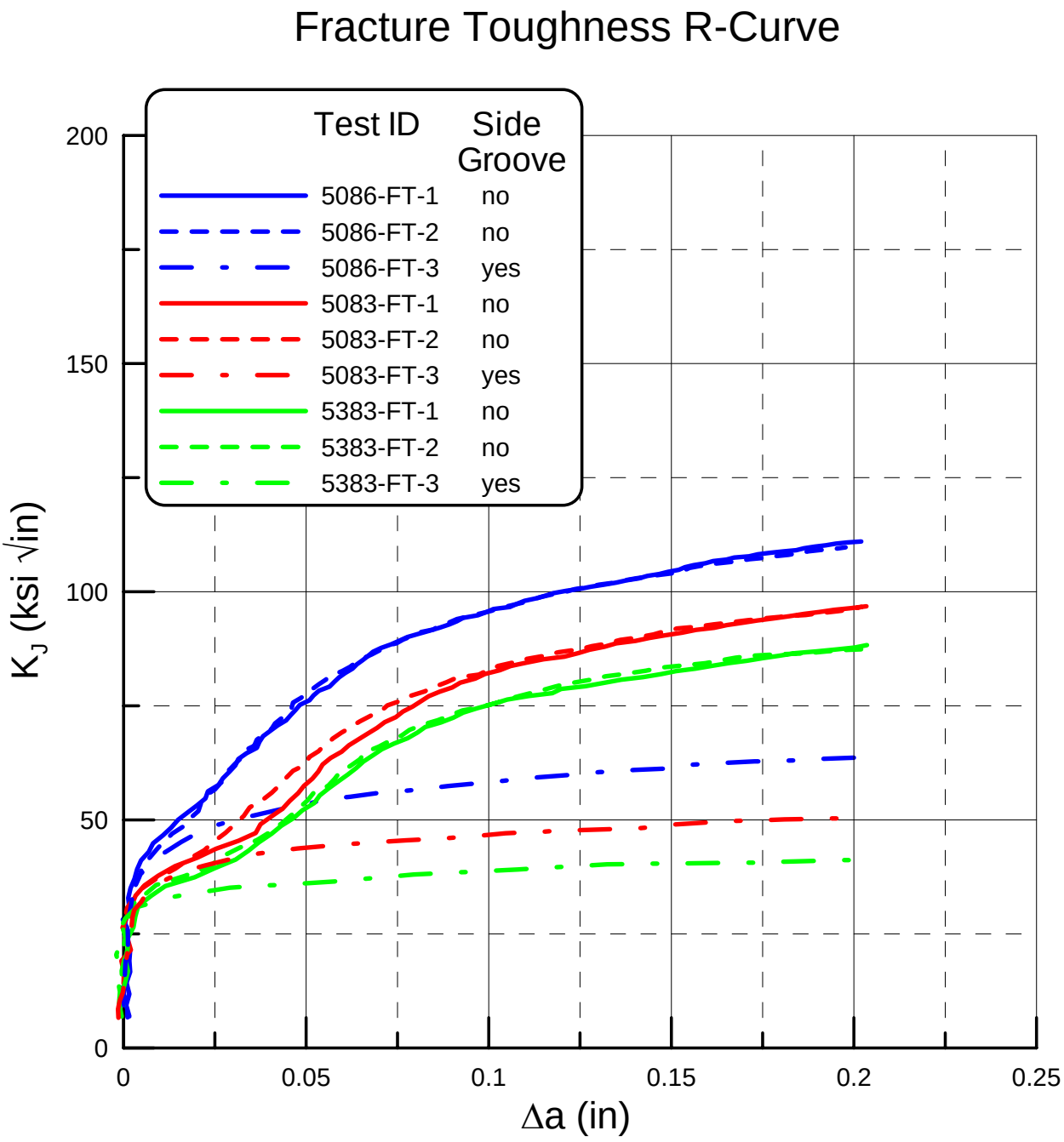

FIGURE 3.5.3: Non-linear fracture toughness showing ranking of alloys as well as duplicate test results and the effect of side grooves. Equivalent K is plotted.

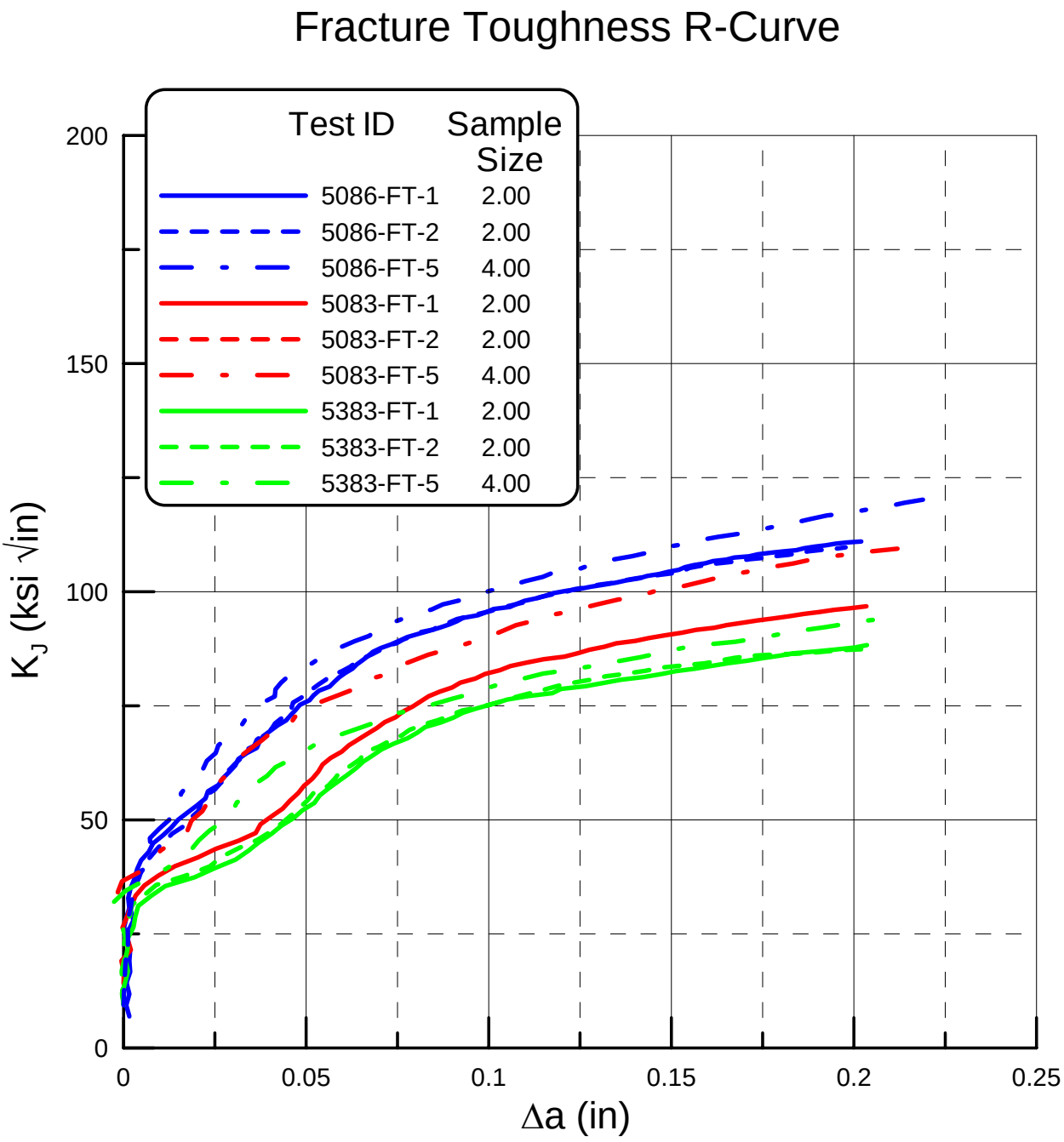

FIGURE 3.5.4: Non-linear fracture toughness showing ranking of alloys as well as duplicate test results and the effect of sample size. Equivalent K is plotted.

SHIP STRUCTURE COMMITTEE LIAISON MEMBERS

LIAISON MEMBERS

American Society of Naval Engineers	Captain Dennis K. Kruse (USN Ret.)
Bath Iron Works	Mr. Steve Tarpy
Colorado School of Mines	Dr. Stephen Liu
Edison Welding Institute	Mr. Rich Green
International Maritime Organization	Mr. Igor Ponomarev
Int'l Ship and Offshore Structure Congress	Dr. Alaa Mansour
INTERTANKO	Mr. Dragos Rauta
Massachusetts Institute of Technology	
Memorial University of Newfoundland	Dr. M. R. Haddara
National Cargo Bureau	Captain Jim McNamara
National Transportation Safety Board - OMS	Dr. Jack Spencer
Office of Naval Research	Dr. Yapa Rajapaksie
Oil Companies International Maritime Forum	Mr. Phillip Murphy
United States Coast Guard Academy	Commander Kurt Colella
United States Merchant Marine Academy	
United States Naval Academy	Dr. Ramswar Bhattacharyya
University of British Columbia	Dr. S. Calisal
University of California Berkeley	Dr. Robert Bea
Univ. of Houston - Composites Eng & Appl.	
University of Maryland	Dr. Bilal Ayyub
University of Michigan	Dr. Michael Bernitsas
Virginia Polytechnic and State Institute	Dr. Alan Brown
Webb Institute	Prof. Roger Compton
Samsung Heavy Industries, Inc.	Dr. Satish Kumar

RECENT SHIP STRUCTURE COMMITTEE PUBLICATIONS

Ship Structure Committee Publications on the Web - All reports from SSC 392 and forward are available to be downloaded from the Ship Structure Committee Web Site at URL:
http://www.shipstructure.org
SSC 445 and below are available on the SSC CD-ROM Library. Visit the National Technical Information Service (NTIS) Web Site for ordering information at URL:
http://www.ntis.gov

SSC Report Number	Report Bibliography
SSC 446	Comparative Study of Ship Structure Design Standards, A. Kendrick, C. Daley 2007
SSC 445	Structural Survivability of Modern Liners, Iversen R. 2005
SSC 444	In-Service Non-Destructive Estimation of the Remaining Fatigue Life of Welded Joints, Dexter R.J., Swanson K.M., Shield C.K. 2005
SSC 443	Design Guidelines for Doubler Plate Repairs on Ship Structures Sensharma P.K., Dinovitzer A., Traynham Y. 2005
SSC 442	Labor-Saving Passive Fire Protection Systems For Aluminum And Composite Construction E. Greene, 2005
SSC 441	Fire Degradation, Failure Prediction And Qualification Methods For Fiber Composites R. Asaro, M. Dao, 2005
SSC 440	Deterioration of Structural Integrity Due to Chemical Treatment of Ballast Water S. Tiku, 2005
SSC 439	Comparative Structural Requirements For High Speed Crafts K. Stone, 2005
SSC 438	Structural Optimization for Conversion of Aluminum Car Ferry to Support Military Vehicle Payload, R.Kramer, 2005
SSC 437	Modeling Longitudinal Damage in Ship Collisions A.J. Brown, JAW Sajdak 2005
SSC 436	Effect of Fabrication Tolerances on Fatigue Life of Welded Joints A. Kendrick, B. Ayyub, I. Assakkaf 2005
SSC 435	Predicting Stable Fatigue Crack Propagation in Stiffened Panels R.J. Dexter, H.N. Mahmoud 2004
SSC 434	Predicting Motion and Structural Loads in Stranded Ships Phase 1 A.J. Brown, M. Simbulan, J. McQuillan, M. Gutierrez 2004